Available online at www.sciencedirect.com
SCIENCE DIRECT®
ELSEVIER
International Journal of Solids and Structures 41 (2004) 7493–7531
INTERNATIONAL JOURNAL OF SOLIDS and STRUCTURES
www.elsevier.com/locate/ijsolstr

Transient analysis of ionic replacements in elastic–plastic expansive clays

Alessandro Gajo [a], Benjamin Loret [b,*]

[a] *Dipartimento di Ingegneria Meccanica e Strutturale, Università di Trento, via Mesiano 77, 38050 Trento, Italy*
[b] *Institut National Polytechnique, Laboratoire Sols, Solides, Structures, Domaine Universitaire, BP 53X, 38041 Grenoble Cedex, France*

Received 23 June 2003; received in revised form 18 February 2004
Available online 18 August 2004

Abstract

Chemically active saturated clays are considered in a two-phase framework. The solid phase contains clay particles, absorbed water and dissolved ions, Na^+, K^+ and Cl^-. The fluid phase, or pore water, contains free water and the same ionic species. Water and ions can transfer between the two phases. In addition, they diffuse through the porous medium. A global understanding of all phenomena, mass transfer, diffusion/advection and deformation is provided. The coupled constitutive equations associated to these phenomena are developed. Emphasis is laid on the electro-chemo-mechanical constitutive equations in an elastic–plastic setting.

A finite element formulation embodying all the above aspects is proposed and simulations of oedometer tests are presented and commented. Of particular interest are the consolidation and swelling that occur during salinization and desalinization of an external reservoir in contact with the specimen, and the more subtle, but important effects of replacing an NaCl pore solution by a KCl pore solution, and conversely.

1. Introduction

Swelling and shrinkage are important issues for natural or engineered soils used in foundations, road pavements, contamination barriers, and petroleum engineering. On the other hand, swelling of bentonite is taken advantage of, so as to decrease soil permeability to contaminants.

Saturation of pore space of swelling clays with an electrolyte is considered here, with water as the solvent and NaCl and KCl as salts in dissolved form. The setting is thus distinct from that in GL [1] where a single salt, namely NaCl, was present so that electrical effects could be disregarded.

While the ultimate goal is to address practical in situ geotechnical problems, the present study is first devoted to simulate tests where the chemical composition of the electrolytic reservoir in contact with a

* Corresponding author. Tel.: +33-4-76-82-52-98; fax: +33-4-76-82-70-00.
E-mail address: benjamin.loret@inpg.fr (B. Loret).

[1] GL stands for Gajo and Loret (2003), LHG for Loret et al. (2002) and GLH stands for Gajo et al. (2002).

0020-7683/$ - see front matter © 2004 Elsevier Ltd. All rights reserved.
doi:10.1016/j.ijsolstr.2004.02.055

laboratory specimen is changed, inducing swelling or shrinkage. Simulations aim at qualitatively and quantitatively reproducing experimental data. Focus is on the relations between reservoir concentration and specimen swelling and shrinkage. In fact, the very nature of the ionic species present in the bath, as well as the mechanical conditions, matter as far as the amplitudes of the volume changes are concerned. KCl has been shown to stiffen clay considerably more than NaCl, Fig. 1. Therefore the model should be able to account for the individual effects of salts. While cycles of chemical and mechanical loadings are simulated, irreversible strains develop, and an elastic analysis would be inadequate. The elastic–plastic constitutive setting used here has been developed in GLH. In order to address the finite element simulations of the tests, further constitutive aspects need to be considered. Indeed, several types of coupling are at work in the simulations. They involve

Elastic and plastic couplings: the mass-contents of absorbed water and cations have a strong influence on the elastic and elastic–plastic properties of solid phase.
Mass transfers between the phases: the physico-chemical reactions picturing exchange of water and cations between the fluid phase and the clay clusters are essential ingredients to the mechanical couplings above.

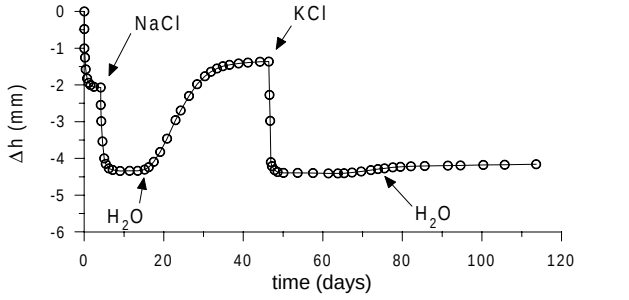

(a) Experimental data on Bisacciaclay,Di Maio and Fenelli (1997).

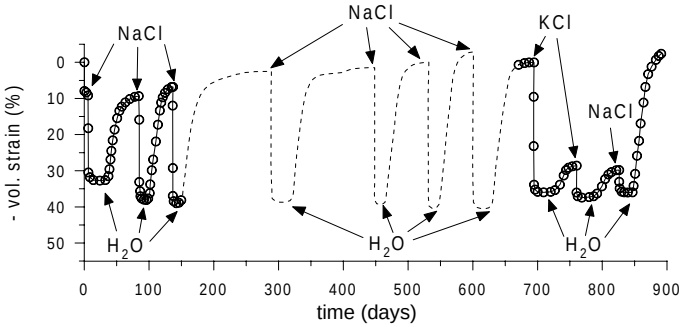

(b) Experimental data on Ponza bentonite,Di Maio (1998).

Fig. 1. Successive replacements of pore solution by NaCl and KCl saturated solutions during oedometric tests at constant vertical stress of 40 kPa. Evolution of (a) the settlement and (b) the volumetric (or axial) strain. The replacement of cations initially present in Ponza bentonite by cations Na^+ is slow, progressive and requires several cycles to get steady. The *reversible* or *irreversible* character of the material response to a chemical loading is difficult to be defined because it involves a number of physical aspects, as well as microstructural features of the clays. For example, Figure (b) shows that saturation of the fresh reservoir by KCl results in about the same consolidation as that induced by NaCl. However, later refreshment of the reservoir implies a very small swelling. The phenomenon is due to displacement of ions Na^+ by ions K^+, and this stiffens notably the material behaviour. The initial volume is recovered only if a complete symmetric chemical loading path is imposed, that is H_2O–NaCl–H_2O–KCl–H_2O–NaCl–H_2O.

Diffusion couplings: the constitutive equations for generalized diffusion involve seepage of water, water-advected diffusion of ionic species and electrical flow through the porous medium. Couplings between these flows are introduced by osmotic efficiency whose intensity strongly decreases with salt concentration, by ionic mobilities and electro-osmotic conductivity.

Therefore, the analysis encompasses both the hydrogeologic point of view which addresses the two last aspects only, no deformation being accounted for, and the classic geomechanical perspective where only hydro-mechanical coupling is accounted for.

Saturated clay is viewed as a porous deformable continuum consisting of two overlapping phases, each phase containing several species. Phase identification follows a kinematic criterion and attributes the absorbed water to the solid phase based on the affinity of their velocities, Hueckel (1992).

The electro-chemo-mechanical elastic–plastic constitutive equations involve the species of the solid phase (the clay platelets) but treat the fluid phase as a whole. The species of the latter only diffuse through the porous medium, obeying generalized diffusion equations. Clay platelets are surrounded by a fictitious membrane. This membrane is permeable to water and ionic species at various degrees, but completely impermeable to clay platelets. Electroneutrality is required in each of the two phases.

In the double porosity models applied to fractured rocks, fluid exchanges between two types of cavities, pores and fractures, depending on the relative pressures. Here water and cations transfer between the solid and the fluid phases. In both frameworks, these exchanges, or transfers, can be viewed as introducing internal memory effects.

Attention is paid to symmetries when formulating the constitutive equations for mass transfer, generalized diffusion, chemo-elasticity and chemo-elastoplasticity. However, the finite element formulation gives rise to matrices with non-symmetric profiles. Non-symmetry of the global diffusion and stiffness arises due to the involment of couplings of different natures, even if each of them, taken individually, would lead to symmetry. Indeed, the generalized diffusion law obeys Onsager reciprocity principle, and plasticity can be associative. The cure of spurious oscillations due to advection-diffusion by an implicit SUPG method introduces another source of non-symmetry in the effective diffusion matrix. More symmetric profiles might be envisaged using a lagrangian approach to tackle the incompressibility constraint and the electroneutrality condition if required, e.g. Levenston et al. (1998). The price to pay is a larger size of matrices, with two lagrangians as additional unknowns.

As for the geomechanical models of the issues addressed here, the ones we are aware of use too strong restrictions to qualify for the tests envisaged, in as far they consider deformable materials which are linear elastic, and also neglect non-linear couplings. While valuable, as it allows for analytical developments, a linear elastic approach is really limited in the interpretation of laboratory tests or field events. To our knowledge no one of the works mentioned below has provided a calibration of their parameters using either laboratory or field instrumented data, nor have been simulations of the controlled situations presented. The only case where the elastic assumption can be used with confidence concerns strongly overconsolidated materials. In fact, it has been argumented in GL, and it is reiterated here, that couplings between elastic–plastic properties and chemistry are strong, and most experimental paths that we have simulated contain at least a portion of plastic loading.

Barbour and Fredlund (1989), Kaczmarek and Hueckel (1998), Smith (2000) consider essentially one-dimensional linear elastic models intended to analyze the effect of organic contaminant diffusion on a deformable medium. Sherwood (1993) has formulated a poroelastic constitutive behaviour referred to as *inert*, where the solid particles constitute the solid phase but the fluid phase contains several species, water and salts. The model has been used in a petroleum engineering context. Bennethum and Cushman (1999) and Murad (1999) have addressed the transfer of water into interlamellar space in clays through a two- or three-spatial scale modeling using homogenization schemes. This type of approach entails a substantial number of constitutive assumptions, requiring sophisticated identification procedures. Geomechanical

instances where electro-chemical couplings are key phenomena, like in modelling of electrokinetic remediations of metal-contaminated soils, have so far considered non-deformable soils, e.g. Yeung (1990) and Yeung and Datla (1995).

Generalized diffusion and diffusion couplings follow quite a similar framework for clays and articular cartilages, Simon et al. (1998), Levenston et al. (1998) and Huyghe and Janssen (1999). Electrical interactions between ions and negatively charged clay platelets and proteoglycans play a key role on the deformability of clays and cartilages respectively. However, the completely different constitutions of the solid phases, clay minerals on one side, macromolecules of collagen and proteoglycans on the other side, imply the elastic coupling to be sensibly different, e.g. Loret and Gajo (2004).

The paper is organized as follows. Basic entities pertaining to the two-phase/multi-species framework used here are defined in Section 2, and the local balance equations are stated in view of future use in the finite element simulations. The mass transfer equations, generalized diffusion equations and the elastic–plastic constitutive equations are motivated by satisfaction of a general dissipation inequality that naturally highlights electro-chemo-mechanical couplings, Section 3. Mass transfer is viewed as a physico-chemical reaction. The generalized diffusion equations couple hydraulic, diffusion and electrical effects. The influences of these couplings in the balance equations are highlighted. For comprehensiveness, the elastic and elastic–plastic constitutive equations developed in GLH are summarized in Section 4.

The weak form of the field equations and the time-integration procedure to solve the highly non-linear matrix equations through a finite element procedure are provided in Section 5. Non-linearity is contributed by all aspects of the model, *inter alia* chemical potentials and osmotic efficiency are strongly non-linear functions of salt concentration, and elasto-plasticity introduces another type of strong non-linearity. The choice of the eight primary variables, and associated field equations, is motivated by the general perspective of this electro-chemo-mechanical analysis in fluid-saturated porous media. In particular, they have to provide sufficient information to define at each time step the elastic–plastic state of the two-phase medium. These primary variables are the solid displacement vector, the fluid pressure, the concentrations of Na^+, K^+ and Cl^- in the fluid phase, the mass-contents of absorbed water and Na^+ in the solid phase, and the electrical potential.

Simulations of documented oedometer tests evidence the influences of the various couplings in transient initial and boundary value problems, Section 6. Notice however that neither the formulation nor the parameter identification are restricted to this one-dimensional setting. Attention is paid to the simulations of shrinking and swelling that accompany the changes of salinity of the reservoir, and therefore of the pore electrolyte. In agreement with data, Di Maio and Fenelli (1997); Di Maio (1998), replacement of a Na-dominated pore solution by distilled pore water produces a quite different swelling strain than if the replacement were made from a K-dominated pore solution.

Notation: Compact or index tensorial notation will be used throughout this work. Tensor quantities are identified by boldface letters. $\mathbf{I} = (I_{ij})$ is the second order identity tensor (Kronecker delta). Symbols '·' and ':' between tensors of various orders denote their inner product with single and double contraction respectively. tr denotes the trace of a second order tensor, dev its deviatoric part and div is the divergence operator. Unless stated otherwise, the convention of summation over repeated indices does *not* apply.

2. The two-phase framework

2.1. General framework

We consider a two-phase porous medium. Each phase is composed of several species. The *solid phase S* contains five species: clay particles denoted by the symbol c, absorbed and adsorbed water (w), ions sodium

Na^+, potassium K^+, chloride Cl^-. The *fluid phase W* contains four species: pore water and ions sodium, potassium and chloride.

The clay clusters are surrounded by a fictitious membrane which is a priori impermeable to clay particles only: clay suspensions are out of the realm of this study. Thus the mass of clay in the solid phase, obtained by aggregation of clay clusters, is constant. The membrane could serve also as a barrier for anions or non-exchangeable cations. A species in a phase is referred to by two indices, the index of the species and the index of the phase. Several sets of species with specific properties are introduced namely:

- species in the solid phase $S = \{c, w, Na^+, K^+, Cl^-\}$;
- species in the fluid phase $W = \{w, Na^+, K^+, Cl^-\}$;
- species that can cross the membrane $S^{\leftrightarrow} = W^{\leftrightarrow} = W = \{w, Na^+, K^+, Cl^-\}$;
- ionic species in the fluid phase $W^{\pm} = \{Na^+, K^+, Cl^-\}$.

The main assumptions which underly the two-phase multi-species model follow the *strongly interacting* model of Bataille and Kestin (1977), namely,

(H1) The mass balance is required for each species. Mass balance for each phase is obtained via mass balances of the species it contains.
(H2) Momentum balance is required for the mixture as whole. Species in the fluid phase are endowed with their own velocities so as to allow them to satisfy their own balance of momentum and to diffuse *in* their phase, possibly with electrical effects.
(H3) The velocity of any species in the solid phase is that of the latter, $\mathbf{v}_{kS} = \mathbf{v}_S$, $\forall k \in S$, and therefore their balance of momentum is not required explicitly, but accounted for by the balance of momentum of the mixture. Water and ions of the solid phase *transfer* to and from the fluid phase.
(H4) In the fluid phase, the pressure is assumed to be uniform across all species, $p_{kW} = p_W$, $\forall k \in W$. In contrast, absorbed species in the solid phase are endowed, through specific constitutive equations, with their own intrinsic pressure.
(H5) Electroneutrality is required in each phase separately. In the solid phase, negatively charged clay particles require the presence of the absorbed cations.

In the solid phase, the pressures attributed to the phase and to the species in that phase are not set a priori as equal. At variance with assumption (H5), Levenston et al. (1998) consider a single electroneutrality condition for biological tissues. In fact, the situation of polymer gels and hydrated biological tissues presents some similarity with that of clay: the solid skeleton structured primarily by collagen fibrils contain negatively charged proteoglycans. But Levenston et al. (1998) consider that the cations are part of the fluid phase, so that the phases in their study are not neutral. In contrast, we make a distinction between absorbed cations which are kinematically tied to the clay particles (H3) and cations in the fluid phases which are endowed with their own velocities (H4).

Assumptions (H1)–(H2) are compatible with the usual finite element alternatives which consist in

- either imposing the balance of momentum of the whole mixture and the balance of mass of the fluid phase (or some equivalent scalar condition), the solid displacement and fluid pressure being part of the primary unknowns;
- or imposing the balances of momentum of both solid and fluid phases, the fluid displacement replacing the fluid pressure as a primary unknown.

Of course the presence of ionic species and electrical effects increases the list of primary variables and associated field equations.

2.2. Basic entities

A key entity that accounts for the chemical properties of species k of phase K is the *electro-chemical potential* which can be mass-based and denoted μ^{ec}_{kK} [unit m^2/s^2], or mole-based and denoted $g^{(\mathrm{ec})}_{kK}$ [unit m^2 kg/s^2/mol], that is $g^{(\mathrm{ec})}_{kK} = m^{(M)}_k \mu^{(\mathrm{ec})}_{kK}$, with $m^{(M)}_k$ molar mass of species k, e.g. $m^{(M)}_w = 18$ gm. Let the initial volume of the porous medium be V_0 and let $V = V(t)$ be its current volume (Fig. 2). The incremental work done by the total stress $\boldsymbol{\sigma}$ in the incremental strain $\delta\epsilon$ of the solid phase and by the electro-chemical potentials μ^{ec}_{kK} during the addition of mass δm_{kK} of the species k to the phase K (or by the electro-chemical potentials g^{ec}_{kK} during the addition/subtraction of δN_{kK} moles) can be cast in either form

$$\delta\Psi = \boldsymbol{\sigma} : \delta\epsilon + \sum_{k,K} \mu^{\mathrm{ec}}_{kK}\delta m_{kK} \iff \delta\Psi = \boldsymbol{\sigma} : \delta\epsilon + \sum_{k,K} g^{\mathrm{ec}}_{kK}\delta\frac{N_{kK}}{V_0}. \tag{2.1}$$

Summation extends to all $k \in S^{\leftrightarrow} = W^{\leftrightarrow} = W$ and $K = S, W$, since the mass of the clay particles is constant. The m_{kK}'s are the fluid mass-contents per unit initial volume of the porous medium [unit kg/m^3].

The constitutive equations will be phrased in terms of mass-based (electro-)chemical potentials, with the mass-contents as independent variables. However, data are available for mole-based free enthalpies of formation. Therefore, use will be made of the entities best appropriate to the context.

The classical formula of the chemical potential of the species k in the fluid phase W, e.g. Haase (1990, Chapters 2–5), identifies

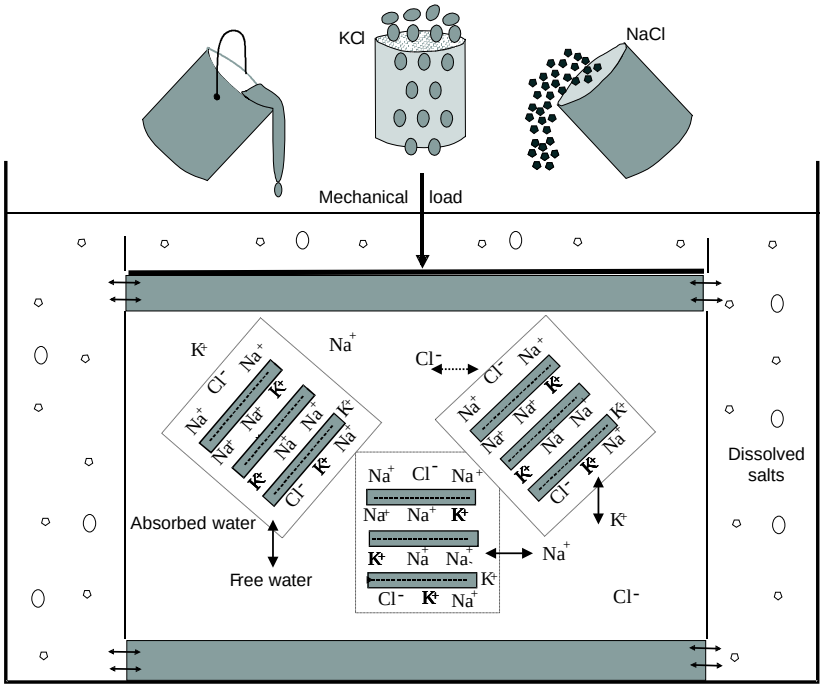

Fig. 2. Schematic of a chemo-mechanical experiment on a heteroionic clay. The pore water is in contact with a large reservoir whose chemical composition is controlled. In the sample submitted to a variable mechanical load in terms of stress or strain, the solid phase (clay clusters structured by negatively charged particles with attached absorbed water and ions) is in contact with the fluid phase (pore water with dissolved salts). Water and ions absorbed in the solid phase are exchanged with their counterparts in pore water depending on their respective contents and on mechanical conditions.

- a purely mechanical contribution which involves the *intrinsic pressure* of the fluid phase p_W, and the intrinsic density ρ_k or *molar volume of the species* $v_k^{(M)}$, and
- a chemical contribution which accounts for the *molar fraction* x_{kW} of the species k in phase W.

For charged species in presence of the electrical potential ϕ^W [unit Volt $=$ kg m^2/s^3/A], the electro-chemical potentials involve in addition an electrical contribution. Moreover, soluble species develop also a configurational energetic property measured by their free enthalpy of formation g_{kW}^0. As for the species within the solid phase S, the mechanical contribution to the electro-chemical potential of species k is assumed to involve its intrinsic mean-stress p_{kS} to be defined by constitutive relations. In integral form,

$$m_k^{(M)}\mu_{kK}^{\mathrm{ec}} = g_{kK}^{\mathrm{ec}} = g_{kK}^0 + \int v_k^{(M)} dp'_{kK} + RT\,\mathrm{Ln}\,x_{kK} + \zeta_k F\phi^K, \tag{2.2}$$

with $p_{kW} = p_W$, $k \in W$. The integration above is performed from a reference state, say ($p_W = p_W^0$, $x_{kW} = 1$, $\phi^W = 0$), to the current state. Therefore, g_{kW}^0 serves as the mole-based value of the chemical potential in the reference state. In these formulas, $R = 8.31451$ J/mol/°C is the universal gas constant, and T (°C) the absolute temperature. The electrical contribution to the chemical potentials is introduced through the valence ζ_k and Faraday's equivalent charge $F =$ Avogadro number $\times$ charge of an electron $= 96487$ Coulomb/mole (1 Coulomb $=$ 1 A s). By convention, $\zeta_w = 0$.

One of the principal tasks in building a theory of deformable porous media is to link the change of pore space to the mass of pore liquid flowing in or out of the representative volume element. This description is more complex when reactions take place, resulting in generation or disappearance of mass. We shall define below different measures of mass changes and volume changes that will be used in the constitutive and field equations.

The *molar fraction* x_{kK} of the species k in phase K is defined by the relative ratio of the mole number N_{kK} of that species within the phase K, namely

$$x_{kK} = \frac{N_{kK}}{\sum_{l\in K} N_{lK}} \quad \text{with} \ \sum_{k\in K} x_{kK} = 1, \ K = S, W. \tag{2.3}$$

The current volume of the species k of phase K is denoted by V_{kK} and the current volume of the phase K by V_K. Then the *volume fraction* of the species k of the phase K is defined as $n_{kK} = V_{kK}/V$ while the volume fraction of the phase K is $n_K = V_K/V = \sum_{k\in K} n_{kK}$ and $n_S + n_W = 1$. On the other hand, *volume-contents* $v_{kK} = V_{kK}/V_0 = n_{kK}V/V_0$ for the species k of phase K and $v_K = V_K/V_0 = n_K V/V_0$ for the phase K refer to the initial total volume V_0. The *mass-contents* m_{kK} per unit initial volume V_0 of the species k of phase K, and m_K of the phase K, are obtained from the volume-contents v_{kK} and *intrinsic* mass densities ρ_k:

$$m_{kK} = \frac{M_{kK}}{V_0} = \frac{N_{kK}m_k^{(M)}}{V_0} = \rho_k v_{kK}, \quad m_K = \frac{M_K}{V_0} = \sum_{k\in K} m_{kK}. \tag{2.4}$$

With (2.4), the molar fractions x_{kK} can be expressed in terms of the mass-contents. For incompressible species, the mass- and volume-contents are one and the same variables, and, although transfer and constitutive equations are phrased in terms of mass-contents, the use of volume-contents may occasionally simplify the notations.

The *apparent* density of the species k in the porous medium, namely $\rho^{kK} = n_{kK}\rho_k$, and the *apparent* density of the phase K, namely $\rho^K = \sum_{k\in K} \rho^{kK}$, refer to the volume of porous medium. The molar volume $v_k^{(M)}$ and molar mass $m_k^{(M)}$ of the species k are linked by the intrinsic density ρ_k, namely $m_k^{(M)} = \rho_k v_k^{(M)}$ (no summation on k), so that, in incremental form, the mechanical contribution to the mass-based potential is $\delta p_W/\rho_k$ for the species k of the fluid phase and $\delta p_{kS}/\rho_k$ for the species k of the solid phase. Note that the density of any species is assumed to be one and the same in both solid and fluid phases.

We will also need the non-dimensional concentration c_{kW} which is the volume fraction referred to the fluid phase rather than to the porous medium, namely [2]

$$c_{kW} = \frac{\text{volume of species } k \text{ of fluid phase}}{\text{volume of fluid phase}} = \frac{V_{kW}}{V_W} = \frac{n_{kW}}{n_W} = \frac{v_{kW}}{n_W}\frac{V_0}{V} = \frac{v_k^{(M)}}{v_W^{(M)}} x_{kW}, \quad k \in W, \tag{2.5}$$

and therefore $\sum_{k\in W} c_{kW} = 1$. The *molar volume* of the fluid phase is $v_W^{(M)} = \sum_{k\in W} x_{kW} v_k^{(M)}$.

Under standard conditions of temperature and pressure, the maximum mass of NaCl dissolved in one liter of distilled water is 360 gm, that is 6.15 moles, since $m_{\mathrm{Na}}^{(M)} = 23$ gm and $m_{\mathrm{Cl}}^{(M)} = 35.5$ gm,[3] corresponding to the molar fraction $x_{\mathrm{NaW}}^{\mathrm{sat}} = 0.091$, i.e. $x_{wW}^{\mathrm{Na-sat}} = 0.819$. The molar volume of dissolved salt varies from 17.6 cm^3 at low molarity of 0.25 mol/l to 21.3 cm^3 at high molarity of 5.142 mol/l. Here, we admit a fixed value of $v_{\mathrm{NaCl}}^{(M)} = 20$ cm^3. The molar volume of the fluid phase varies from 18 cm^3 for distilled water to $0.9 \times 18 + 0.1 \times v_{\mathrm{NaCl}}^{(M)} = 18.2$ cm^3, which gives a saturated salt concentration $c_{\mathrm{NaW}}^{\mathrm{sat}} = 0.10$, or equivalently $c_{\mathrm{NaW}}^{\mathrm{sat}}/v_{\mathrm{NaCl}}^{(M)}$ equal to 5 moles, or also 115 gm of Na^+ per liter of solution (≡ fluid phase). The maximum mass of KCl dissolved in one liter of distilled water is 342 gm, that is 4.58 moles, since $m_{\mathrm{K}}^{(M)} = 39.1$ gm. Admitting also a molar volume of dissolved salt of $v_{\mathrm{KCl}}^{(M)} = 20$ cm^3, the above figures become $x_{\mathrm{KW}}^{\mathrm{sat}} = 0.071$, i.e. $x_{wW}^{\mathrm{K-sat}} = 0.858$, $v_W^{(M)} = 18.15$ cm^3, $c_{\mathrm{KW}}^{\mathrm{sat}} = 0.078$, or equivalenty $c_{\mathrm{KW}}^{\mathrm{sat}}/v_{\mathrm{KCl}}^{(M)}$ equal to 3.91 moles, or also 153 gm of K^+ per liter of solution. If the salts were dissolved together, the above saturated values would vary, but saturation in the presence of the two salts does not occur in the experimental data to be simulated.

Two additional phase entities of physical importance in electrolytes are the electrical density and the electrical current density. The latter definition is deferred to Section 2.5. In phase K, the *electrical density* I_{eK} [unit Coulomb/m^3] can be expressed inter alia in terms of mole numbers, molar fractions, or mass-contents,

$$I_{eK} = \frac{F}{V}\sum_{k\in K} \zeta_k N_{kK} = F\frac{N_K}{V}\sum_{k\in K} \zeta_k x_{kK} = F\frac{V_0}{V}\sum_{k\in K} \zeta_k \frac{m_{kK}}{m_k^{(M)}}, \tag{2.6}$$

and, in addition, for the fluid phase, in terms of concentrations as

$$I_{\mathrm{e}W} = n_W \sum_{k\in W} \zeta_k \frac{c_{kW}}{v_k^{(M)}}. \tag{2.7}$$

The fulfillment of *electroneutrality* in phase K is simply $I_{eK} = 0$.

Both the solid and fluid phases are assumed to be electrically neutral. The electroneutrality condition sets a minimal admissible value for the molar fractions of the absorbed cations, especially when the pore solution is distilled water: then at equilibrium, the molar fraction of absorbed water overweights the other molar fractions. However, electroneutrality implies

$$N_{\mathrm{Na}S} + N_{KS} = -\zeta_c N_{cS} + N_{\mathrm{Cl}S} > 0 \iff X \equiv x_{\mathrm{Na}S} + x_{\mathrm{K}S} = -\zeta_c x_{cS} + x_{\mathrm{Cl}S} > 0. \tag{2.8}$$

2.3. Electro-chemical energy of the fluid phase

In order to define the mechanical constitutive equations of the porous medium, the electro-chemical effects in pore water will be isolated. Using the Gibbs-Duhem relation, Section 2.3 in GLH, the differential of the electro-chemical energy of the fluid phase per initial unit volume of the porous medium can be cast in the form,

[2] Traditional analyses make use of the concentration measured in mol/volume of solution, that is of $c_{kW}/v_k^{(M)}$, or in mass/volume of solution, that is $\rho_k c_{kW}$.

[3] The following values of molar volumes have been used: $v_{\mathrm{Na}}^{(M)} = 3$ cm^3/mole, $v_{\mathrm{K}}^{(M)} = 13$ cm^3/mole, $v_{\mathrm{Cl}}^{(M)} = 17$ cm^3/mole, and hence $\rho_{\mathrm{Na}} = 7.66$ kg/l, $\rho_K = 3$ kg/l, $\rho_{\mathrm{Cl}} = 2.09$ kg/l, $\rho_c = 5.111$ kg/l.

$$\delta\Psi_W = \sum_{k\in W} \mu_{kW}^{(\mathrm{ec})}\delta m_{kW} - p_W \delta v_W, \tag{2.9}$$

the electrical contribution vanishing due to electroneutrality of the fluid phase, Eqs. (2.6), (2.7).

2.4. Incompressibility constraint

A situation of particular interest arises when all species are incompressible, $\delta\rho_k = 0$, $\forall k$. Then, there exists a relation between the variables $\{\epsilon, v_W, \{v_{kS} = m_{kS}/\rho_k, k \in S^{\leftrightarrow}\}\}$. Indeed, the volume change of the porous medium is then equal to the sum of the changes of volume-contents of the individual species, so that

$$\delta v_W = \delta \operatorname{tr}\epsilon - \sum_{k\in S^{\leftrightarrow}} \delta v_{kS}. \tag{2.10}$$

2.5. Balance equations

The mass balance equations will be written for all the species in the fluid phase but water, and for the fluid phase as a whole. To simplify the analysis, the species are assumed to be incompressible. Balance of momentum will be required for the mixture as whole.

2.5.1. Mass, volume fluxes and electrical current density

Balance equations are phrased in terms of several fluxes. Because of the incompressibility of the species, mass fluxes and volume fluxes can be viewed as entities that differ only by their units. The *mass flux* $\mathbf{M}_{kK}$ and the associated *volume flux* $\mathbf{J}_{kK}$ of the species k of phase K through the solid skeleton are defined as,

$$\mathbf{M}_{kK} = \rho_k \mathbf{J}_{kK} = \rho^{kK}(\mathbf{v}_{kK} - \mathbf{v}_S). \tag{2.11}$$

Due to assumption (H3), only the fluxes of the species in the fluid phase are not zero. The sum of the fluxes $\mathbf{J}_{kW}$ provides the volume averaged flux $\mathbf{J}_W$ of fluid phase through the solid skeleton,

$$\mathbf{J}_W = \sum_{k\in W} n_{kW}(\mathbf{v}_{kW} - \mathbf{v}_S). \tag{2.12}$$

The diffusive flux of a species with respect to water in the fluid phase is denoted as $\mathbf{J}^d_{kW}$,

$$\mathbf{J}^d_{kW} = n_{kW}(\mathbf{v}_{kW} - \mathbf{v}_{wW}). \tag{2.13}$$

The *electrical current density* $\mathbf{I}_{eK}$ in phase K [unit A/m^2] is defined as the sum of constituent velocities weighted by their valences and molar densities,

$$\mathbf{I}_{eK} = F\sum_{k\in K} \zeta_k \frac{N_{kK}}{V}\mathbf{v}_{kK}. \tag{2.14}$$

On comparing $(2.6)_2$ and (2.14), a uniform velocity for all species of a phase satisfying electroneutrality is seen to be a sufficient condition for the electrical current density to vanish in that phase, therefore $\mathbf{I}_{eS} = \mathbf{0}$. If electroneutrality is assumed in the fluid phase, $\mathbf{I}_{eW}$ may be viewed as a sum of either interphase or diffusive fluxes, namely

$$\mathbf{I}_{eW} = F\sum_{k\in W} \frac{\zeta_k}{v_k^{(M)}}\mathbf{J}_{kW} = F\sum_{k\in W} \frac{\zeta_k}{v_k^{(M)}}\mathbf{J}^d_{kW}. \tag{2.15}$$

2.5.2. Balances of masses

The change of mass of a species is due a priori to both *transfer* through the fictitious membrane, i.e. a physico-chemical reaction, and *diffusion*. The changes in the species of the solid phase are purely reactive, and they are due to transfer through the membrane, between the solid and fluid phases, of water and ionic species. On the other hand, the species of the fluid phase may also undergo mass changes by exchanges (diffusion) with the outside, so that

$$\frac{\delta m_{kW}}{\delta t} = -\frac{\delta m_{kS}}{\delta t} - \operatorname{div} \mathbf{M}_{kW}, \quad k \in W. \tag{2.16}$$

Here the symbol $\delta/\delta t$ means derivative following the solid phase. The implied balance of mass of the species k in fluid phase may be phrased in terms of the concentration c_{kW}, Eq. (2.5), and of the rate of n_W given by Eq. (A.9) of GL, namely, neglecting the spatial heterogeneity of ρ_k,

$$n_W \frac{\delta c_{kW}}{\delta t} + c_{kW} \operatorname{div} \mathbf{v}_S + \operatorname{div} \mathbf{J}_{kW} + \sum_{l \in S^{\leftrightarrow}} (I_{kl} - c_{kW}) \frac{\delta v_{lS}}{\delta t} = 0, \quad k \in W. \tag{2.17}$$

Eq. (2.17) indicates that the change of salt concentration is due to change of volume of solid skeleton, diffusion of species through the porous medium, and transfer of all species between the two phases, with appropriate weights and signs. A comparison, centered on the balance equation (2.17), of the present framework with hydrogeological approaches is briefly sketched in Appendix E.

As another consequence of (2.16), if electroneutrality is assumed in both the solid and fluid phases, $\mathbf{I}_{eW}$ defined by (2.14), or (2.15), is divergence free as shown in Appendix A,

$$\operatorname{div} \mathbf{I}_{eW} = 0. \tag{2.18}$$

For incompressible species, the change of volume of the porous medium is equal and opposite to the volume change of the fluid phase that diffuses through this medium,

$$\operatorname{div} \mathbf{v}_S + \operatorname{div} \mathbf{J}_W = 0. \tag{2.19}$$

2.5.3. Balance of momentum

Under quasi-static loading and with the sole gravity $\mathbf{g}$ with intensity g as body force, the balance of momentum of the porous medium as a whole is, e.g. Eringen and Ingram (1965),

$$\operatorname{div} \boldsymbol{\sigma} + \rho \mathbf{g} = \mathbf{0}, \tag{2.20}$$

where ρ is the density of the porous medium, i.e. $\rho = \sum_{k,K} \rho^{kK} = \sum_K \rho^K$.

3. The global picture: deformation, mass transfer, diffusion and electrical flow

In the absence of thermal effects, starting from the statements of balance of mass for each species, and balance of momentum and of energy for the phases, the Clausius-Duhem inequality for the mixture as a whole can be cast in a format (see Eq. (3.6) in GLH) that highlights mechanical, transfer and diffusion contributions. These contributions will be required to be positive individually,

$$\begin{cases} \delta D_1 = -\delta \Psi + \boldsymbol{\sigma} : \delta \epsilon + \sum_{k,K} \mu_{kK} \delta m_{kK} \geqslant 0, \\ \delta D_2/\delta t = -\sum_{k \in S^{\leftrightarrow}} (\mu^{\mathrm{ec}}_{kS} - \mu^{\mathrm{ec}}_{kW}) \hat{\rho}^{kS} \geqslant 0, \\ \delta D_3/\delta t = -\sum_{k \in W} (\nabla \mu^{\mathrm{ec}}_{kW} - \mathbf{b}_{kW}) \cdot \mathbf{M}_{kW} \geqslant 0. \end{cases} \tag{3.1}$$

The chemo-hyperelastic behaviour will be constructed in order for the first term δD_1 to exactly vanish, Section 4.1. Due to phase electroneutrality, the electrical field does not work, and this has lead to the

electro-chemical potentials in δD_1 to be replaced by the chemical potentials. Consequently, the elastic constitutive relations do not depend directly on the electrical field.

Satisfaction of the second and third inequalities motivates generalized transfer equations and generalized diffusion equations respectively. These are elaborated below for electrolytic solutions. Only acceleration of gravity will be considered, i.e. all body force densities $\mathbf{b}_{kW}$ are equal to $\mathbf{g}$.

3.1. Interphase mass transfer as a chemical reaction

Transfer of ions and water is now viewed as a chemical reaction, which does not alter the electroneutrality of the solid phase.

The amount of chloride anions in the solid phase is certainly small due to the presence of the negatively charged clay platelets. So, we may assume that the membrane is impermeable to chloride anions, or even that the number of moles of chloride anions in the solid phase is negligible, $N_{\mathrm{Cl}S} \simeq 0$. Therefore, from (2.8), the total number of exchangeable cations [4] N_{ex} in the solid phase turns out to be constant. Consequently, a single variable is sufficient to describe the variation of the number of cations in the solid phase. The second variable that describes the state of species in solid phase is the mass-content of water.

According to (2.8), the total and elastic changes in the numbers of moles of cations in the solid and fluid phases are linked by the following relations,

$$\delta N^{(\mathrm{el})}_{\mathrm{Na}S} = -\delta N^{(\mathrm{el})}_{\mathrm{K}S} = -\delta N^{\mathrm{reactive}}_{\mathrm{Na}W} = \delta N^{\mathrm{reactive}}_{KW}, \tag{3.2}$$

where the superscript (el) is intended to imply that the relation is assumed to hold in terms of total numbers of cations, as well as in terms of the reversible change in their number.

Consequences for the relations between changes of (reversible) masses follow from the relation $m^{(\mathrm{el})}_{kK} = m^{(M)}_{k}/V_0 N^{(\mathrm{el})}_{kK}$. Indeed, with (3.2), the inequality $(3.1)_2$ can be phrased equivalently in terms of the (electro-)chemical potentials of water and mass-based (electro-)chemical affinities of the cations. The latter are defined as

$$A_K = A^{\mathrm{ec}}_K = \mu^{(\mathrm{ec})}_{\mathrm{Na}K} - \frac{m^{(M)}_{\mathrm{K}}}{m^{(M)}_{\mathrm{Na}}}\mu^{(\mathrm{ec})}_{\mathrm{K}K} = \frac{1}{m^{(M)}_{\mathrm{Na}}}(g^{(\mathrm{ec})}_{\mathrm{Na}K} - g^{(\mathrm{ec})}_{\mathrm{K}K}), \quad K = S, W. \tag{3.3}$$

The affinities include the difference of free enthalpies of formation between the two cations, which gives rise to an equilibrium constant K_{eq} different from one, as explained in GLH. The resulting transfer relations write,

$$\frac{\delta}{\delta t}\begin{bmatrix} m_{wS} \\ m_{\mathrm{Na}S} \end{bmatrix} = \begin{bmatrix} T_w & T_{w\mathrm{Na}} \\ T_{\mathrm{Na}w} & T_{\mathrm{Na}} \end{bmatrix}\begin{bmatrix} \mu_{wW} - \mu_{wS} \\ A_W - A_S \end{bmatrix}. \tag{3.4}$$

Inequality $\delta D_2 \geqslant 0$ is ensured if the 2×2 coefficient matrix $\mathbf{T}$ is assumed symmetric positive definite, $T_{w\mathrm{Na}} = T_{\mathrm{Na}w}$, $T_w \geqslant 0$, $T_w T_{\mathrm{Na}} - T_{w\mathrm{Na}} T_{\mathrm{Na}w} \geqslant 0$. Uncoupling between the two mass transfers is adopted in the simulations below, i.e. $T_{w\mathrm{Na}} = T_{\mathrm{Na}w} = 0$. It implies that the sole chemical desequilibrium for water does not result in cation transfer, and conversely.

The transfer equations (3.4) involve two characteristic transfer times τ_w and τ_{Na}, which can be displayed by non-dimensionalization,

[4] In fact, in the present analysis, N_{ex} can be considered either as the total number of cations in the solid phase or as the number of exchangeable cations.

$$\tau_w = \frac{m_w^{(M)}}{RT}\frac{\rho_w}{T_w}, \quad \tau_{\mathrm{Na}} = \frac{m_{\mathrm{Na}}^{(M)}}{RT}\frac{\rho_{\mathrm{Na}}}{T_{\mathrm{Na}}}. \tag{3.5}$$

3.2. Generalized diffusion

Inequality $\delta D_3 \geqslant 0$, Eq. (3.1), is ensured by generalization of Darcy's law of seepage through the porous medium, Fick's law of diffusion of ions in the fluid phase, coupled to electrical flow.

3.2.1. Generalized diffusion equations

Using the definition (2.2) and Eqs. $(2.3)_2$, (2.11), (2.13), the dissipation inequality $\delta D_3 \geqslant 0$ can be formally written as the sum of products of a flux times a driving force,

$$\delta D_3/\delta t = -\mathscr{J}^{\mathrm{T}}\mathscr{F} = -\mathbf{J}_W \cdot \mathbf{F}_W - \sum_{k\in W} \mathbf{J}_{kW}^d \cdot \mathbf{F}_{kW}^d - \mathbf{I}_{\mathrm{e}W} \cdot \mathbf{F}_{\mathrm{e}W} \geqslant 0, \tag{3.6}$$

with the vector flux $\mathscr{J}$ and a conjugate vector $\mathscr{F}$,

$$\mathscr{J} = \begin{bmatrix} \mathbf{J}_W \\ \mathbf{J}_{\mathrm{NaW}}^d \\ \mathbf{J}_{\mathrm{K}W}^d \\ \mathbf{J}_{\mathrm{Cl}W}^d \\ \mathbf{I}_{\mathrm{e}W} \end{bmatrix}, \quad \mathscr{F} = \begin{bmatrix} \mathbf{F}_W \\ \mathbf{F}_{\mathrm{Na}W}^d \\ \mathbf{F}_{\mathrm{K}W}^d \\ \mathbf{F}_{\mathrm{Cl}W}^d \\ \mathbf{F}_{\mathrm{e}W} \end{bmatrix} = \begin{bmatrix} \nabla p_W - \rho^W/n_W\mathbf{g} \\ RT/v_{\mathrm{Na}}^{(M)}\nabla \mathrm{Ln}\, c_{\mathrm{Na}W} - (\rho_{\mathrm{Na}} - \rho^W/n_W)\mathbf{g} \\ RT/v_{\mathrm{K}}^{(M)}\nabla \mathrm{Ln}\, c_{\mathrm{K}W} - (\rho_K - \rho^W/n_W\mathbf{g} \\ RT/v_{\mathrm{Cl}}^{(M)}\nabla \mathrm{Ln}\, c_{\mathrm{Cl}W} - (\rho_{\mathrm{Cl}} - \rho^W/n_W)\mathbf{g} \\ \nabla\phi_W \end{bmatrix}. \tag{3.7}$$

In establishing Eq. (3.7), a slight approximation has been done by replacing the ionic molar fraction x_{kW} by the concentration c_{kW} in view of (2.5).

If the material behaviour is assumed isotropic, a generalized law describing flow of pore water through the solid skeleton, diffusion of ions with respect to the free water, and electrical flow, can be introduced in the format,

$$\mathscr{J} = -\mathscr{K}\mathscr{F}, \tag{3.8}$$

with $\mathscr{K}$ a symmetric matrix,

$$\mathscr{K} = \begin{bmatrix} k_{WW} & k_{W\mathrm{Na}}^d & k_{W\mathrm{K}}^d & k_{W\mathrm{Cl}}^d & k_e \\ k_{\mathrm{Na}W}^d & k_{\mathrm{NaNa}}^d & 0 & 0 & k_{\mathrm{Na}e}^d \\ k_{KW}^d & 0 & k_{KK}^d & 0 & k_{Ke}^d \\ k_{\mathrm{Cl}W}^d & 0 & 0 & k_{\mathrm{ClCl}}^d & k_{\mathrm{Cl}e}^d \\ k_e & k_{e\mathrm{Na}}^d & k_{e\mathrm{K}}^d & k_{e\mathrm{Cl}}^d & \boldsymbol{\sigma}_e \end{bmatrix} \tag{3.9}$$

with components

$$\begin{cases} k_{WW} = k_D + \dfrac{k_e^2}{\boldsymbol{\sigma}_e}, \quad k_{ke}^d = n_W c_{kW} u_k^* \operatorname{sgn}\zeta_k, \quad \boldsymbol{\sigma}_{\mathrm{e}} = n_W F \displaystyle\sum_{k\in W^{\pm}} |\zeta_k| \frac{c_{kW}}{v_k^{(M)}} u_k^*, \\ k_{kW}^d = -\omega c_{kW} k_D + \dfrac{k_e}{\boldsymbol{\sigma}_e} k_{ke}^d, \quad k_{kl}^d = n_W v_k^{(M)} c_{kW} \dfrac{D_k^*}{RT} I_{kl}, \quad k, l \in W^{\pm}, \end{cases} \tag{3.10}$$

where $k_D = K_h/(\rho_w g)$. The format used to cast the above coefficients, their signs and the associated terminology are justified in the identification procedure detailed in Loret et al. (2004). In particular, electroneutrality of the fluid phase implies compatibility conditions between the coefficients of the generalized diffusion matrix that are satisfied by (3.10).

3.2.2. Ranges of the diffusion coefficients

In the simpler case of a single anion and a single cation, Yeung (1990) and Mitchell (1993) have provided ranges of values of the above material entities for fine grained soils:

- $K_h \in [10^{-11}, 10^{-6}]$ [unit m/s] is the hydraulic conductivity. In a basic attempt to model the decrease of hydraulic conductivity during swelling, the latter is taken as a function, not of the conventional void ratio, but of the void ratio in this two-phase context, that is $e^{\star} = V_W/V_S$, see GL.
- $\omega \in [0, 1]$, is referred to as (non-dimensional) osmotic efficiency. As an extension of the single salt formulation, ω is taken as function of the total cation concentration (in mol/l), $c^+ \equiv c_{\mathrm{NaW}}/v_{\mathrm{Na}}^{(M)} + c_{\mathrm{K}W}/v_{\mathrm{K}}^{(M)}$, and of water content w. The later is estimated using the specific surface A_s and the half distance b between particle surfaces as $w = 100 b \rho_w A_s$. The specific surface A_s is expressed in terms of the liquid limit using the relation obtained by Farrar and Coleman (1967). The resulting osmotic efficiency decreases quickly as cationic concentration increases at constant water content, and conversely. Data for uncompacted clays show that the osmotic efficiency does not to tend to one at tiny ionic concentrations. This is at variance with the data collected in Mitchell (1991), that represent an upper bound and apply to compacted clays. The following analytical expression of the osmotic efficiency $\omega = \omega(B = b\sqrt{c^+})$ has been adopted:

$$\frac{\omega}{\omega_{\max}} = 1 - \tanh(\beta\langle B - B_0\rangle), \quad \beta = -\frac{\omega'(B_0)}{\omega_{\max}}, \tag{3.11}$$

  where the function $\langle\cdot\rangle$ denotes the positive part of its argument. Positive B_0 values with $\omega_{\max} = 1$ correspond typically to compacted clays. On the other hand, uncompacted clays are characterized by $B_0 = 0$ and $\omega_{\max} < 1$. The values $\omega_{\max} = 0.7$, $\omega'(0) = -0.15$ match the data of Malusis and Shackelford (2002).
- $D_k^{\star} \in [10^{-10}, 2 \times 10^{-9}]$ [unit m^2/s] is the coefficient of *effective* diffusion of ionic species k in soil. The effective diffusion coefficient accounts for the tortuous path that the species have to travel through the porous medium.
- $\boldsymbol{\sigma}_e \in [10^{-2}, 1]$ [unit siemens/m = A/V/m] is the bulk electrical conductivity of soil. It can be viewed as the weighted average in the fluid phase of the ionic mobilities. It is not constant, it assumes a very small but non-zero value for quasi-distilled water and it increases with ionic saturation. It involves only the properties of ions in the fluid phase, as if the path of ions were completely in fluid phase, and the solid phase, where the electrical current density vanishes, does not enter.
- $k_e \in [10^{-9}, 10^{-8}]$ [unit m^2/s/V] is the coefficient of electro-osmotic conductivity. It can be related to the electrical charge of the clay mineral through the Helmholtz–Smoluchowski relation. However, since the value of pH is constant in this analysis, the charge can be considered fixed, k_e has been taken constant.
- $u_k^{\star} \in [3 \times 10^{-9}, 10^{-8}]$ [unit m^2/s/V] is the effective ionic mobility, a diffusive property, that is: the velocity relative to water that the ionic species k can reach under an electrical potential ϕ_W is $-u_k^{\star} \operatorname{sgn}\zeta_k \nabla\phi_W$. The sign of the electrical charge indicates that a cation is moving towards the cathode, while an anion is moving towards the anode, i.e. in the direction of increasing electrical potential. This phenomenon known as *electro-phoresis* is used to densify fine particle suspensions around the anode. In agreement with the usual convention, the electrical current density has a direction opposite to that of electrons. The ionic mobility is linked to the effective diffusion by the Nernst–Einstein relation applied to the soil: $u_k^{\star} = D_k^{\star}|\zeta_k|F/RT$.

Note that the electrical field is generated in order electroneutrality to be satisfied. Indeed, consider an insulator membrane, i.e. $\mathbf{I}_{eW} = \mathbf{0}$, separating two electrolytes containing dissolved NaCl and maintained at the same water pressure. Then Eqs. (3.7)–(3.9) and electroneutrality yield $n_W RT(u_{\mathrm{Na}}^{\star} - u_{\mathrm{Cl}}^{\star})\nabla c_{\mathrm{NaW}} + \boldsymbol{\sigma}_e \nabla\phi_W = 0$. As the ionic mobilities of Na^+ and Cl^- are not equal, a potential difference must develop across the membrane.

The identification of k_{WW} accounts for the fact that measurement of hydraulic conductivity, at uniform ionic concentrations and preventing electrical current $\mathbf{I}_{eW}$, necessarily gives rise to a *streaming potential* $\nabla\phi_W = -k_e/\boldsymbol{\sigma}_e \nabla p_W$, that is, water flows against pore pressure gradient but along the streaming potential gradient. Under these experimental conditions, if the diffusive flow $\mathbf{J}^d_{kW}$ is formally taken as $\omega c_{kW} K_h/\rho_w g \nabla p_W$, the coefficients k^d_{Wk} result as shown in (3.10).

For *electro-osmosis* where the ionic concentrations and pore pressures are uniform, water flows against the electrical potential gradient, that is towards the cathode. This water flow may lead to negative pore pressures (suction) in the cathode region, and thus initiate a consolidation process, Acar et al. (1991). The electro-osmotic conductivity is insensitive to the pore size according to the Helmholtz–Smoluchowski theory, while the hydraulic conductivity decreases with the pore size: therefore, for fine-grained soils, an electrical field is a more efficient tool to displace water than a hydraulic gradient.

3.2.3. An alternative identification of the effective diffusion coefficients

The diffusion coefficients, and ionic mobilities, used above are identified at vanishing pore pressure gradient. For organic solutes, Manassero and Dominijanni (2003) and Malusis and Shackelford (2003) use coefficients of diffusion defined at vanishing water flow $\mathbf{J}_W$. This procedure has been reconsidered for electrolytes. It implies qualitative modifications of the present structure of the generalized diffusion matrix, but the quantitative modifications are quite small, as already observed for organic solutes in Malusis and Shackelford (2003).

A further modification with respect to the present analysis is proposed by these authors, whose main concern is the impermeability to ions of liners made of compacted clays. To reach their goals, they consider that the tortuosity is proportional to $1-\omega$. The consequence is that the effective diffusion coefficients vanish at tiny solute concentrations.

The two modifications suggested by Manassero and Dominijanni (2003) and Malusis and Shackelford (2003) have been coded and tested, but not adopted here, for the following reasons. First, the clays analyzed here are not compacted, and so ω is not expected to reach one, so that the impermeability of the clay specimen to ions is not expected, and in fact not observed in the laboratory experiments of Di Maio (1996). Second, during the simulations of ionic injection reported below, this variable tortuosity model has been observed to imply too large negative pore pressures on the diffusion front, as commented further in Section 6.

4. Elastic and elastic–plastic constitutive equations

The absorption and desorption of water and ionic species to/from the solid phase introduce electro-chemo-mechanical couplings. On the other hand, the mere presence of ions in the water phase does not affect directly the mechanical behavior of the porous medium, they just flow through. Their amount is governed by an equation of mass conservation and a flow equation. Therefore, to develop the electro-chemo-mechanical constitutive equations, the chemical composition of the fluid phase is temporarily ignored. Thus constitutive equations are provided for the following variables:

- a stress–strain couple attached to the mechanical state of the solid phase, namely $(\bar{\boldsymbol{\sigma}}, \epsilon)$;
- as many couples (chemical potential/affinity, mass-content) as there are species that can cross the membrane independently, namely $(\bar{\mu}_{wS}, m_{wS})$ and $(\overline{A}_S, m_{\mathrm{NaS}})$.

Incompressibility of the constituents has eliminated the couple pore pressure p_W—fluid volume-content v_W from the above list, and introduced *effective* quantities denoted by a superimposed bar, namely Terzaghi's effective stress $\bar{\boldsymbol{\sigma}}$, the effective chemical potential $\bar{\mu}_{wS}$, and the effective chemical affinity $\overline{A}_S$,

$$\bar{\boldsymbol{\sigma}} = \boldsymbol{\sigma} + p_W \mathbf{I}, \quad \bar{\mu}_{wS} = \mu_{wS} - \frac{p_W}{\rho_k}, \quad \bar{A}_K = \bar{\mu}_{\mathrm{Na}K} - \frac{m_{\mathrm{K}}^{(M)}}{m_{\mathrm{Na}}^{(M)}} \bar{\mu}_{KK}. \tag{4.1}$$

Use will be made in the sequel of the decomposition of the strain and total and effective stress tensors into their spherical and deviatoric parts, namely

$$\boldsymbol{\epsilon} = \frac{\mathrm{tr}\,\boldsymbol{\epsilon}}{3}\mathbf{I} + \mathrm{dev}\,\boldsymbol{\epsilon}, \quad \boldsymbol{\sigma} = -p\mathbf{I} + \mathbf{s}, \quad \bar{\boldsymbol{\sigma}} = -\bar{p}\mathbf{I} + \mathbf{s}, \tag{4.2}$$

with the two first stress-invariants $p = -\mathrm{tr}\,\boldsymbol{\sigma}/3$ ($\bar{p} = -\mathrm{tr}\,\bar{\boldsymbol{\sigma}}/3$), and $q = (3/2\mathbf{s} : \mathbf{s})^{1/2}$. Note that the transfer relations, Eq. (3.4), are phrased equivalently in terms of total or effective potentials/affinities.

Viewing the transfer of ionic species as a chemical reaction implies electroneutrality to be satisfied automatically in the solid phase.

4.1. Elastic constitutive equations

In absence of ionic transfers, the constitutive equations are designed to reduce to the usual Cam-Clay logarithmic elasticity. Notice however that the dependence of the moduli on the chemical content of the solid phase is accounted for.

In view of extension to the elastic–plastic behaviour, generalized reversible strains will henceforth be denoted by a superscript el. Instances are strains, volume and mass-contents, number of moles. Later, these entities will be decomposed into an elastic (or reversible) part and a plastic (or irreversible) part. Given a reference state, and a process which is reversible from that reference state to the current state, the elastic (or reversible) part of each of above entities is by convention equal to the total entity.

The chemo-elastic potential exhibited in GLH provides hyperelastic constitutive equations. The elastic strain has the form

$$\epsilon^{\mathrm{el}} = \left(\mathrm{tr}\,\epsilon_\kappa^{\mathrm{el}} - \kappa\,\mathrm{Ln}\,\frac{\bar{p}}{\bar{p}_\kappa} \right) \frac{\mathbf{I}}{3} + \frac{\mathbf{s}}{2G}, \tag{4.3}$$

and the effective chemical potential of water $\bar{\mu}_{wS}$ and affinity $\bar{A}_S$ are given, respectively, by Eqs. (3.22) and (3.42) of GLH.

The existence of an elastic potential implies the incremental form of the elastic constitutive equations to be defined by a symmetric 3×3 matrix,

$$\begin{bmatrix} -\delta\bar{p} \\ \delta\bar{\mu}_{wS} \\ \delta\bar{A}_S \end{bmatrix} = \begin{bmatrix} B & B_w & B_{\mathrm{Na}} \\ B_w & \beta_{ww} & \beta_{w\mathrm{Na}} \\ B_{\mathrm{Na}} & \beta_{\mathrm{Naw}} & \beta_{\mathrm{NaNa}} \end{bmatrix} \begin{bmatrix} \delta\,\mathrm{tr}\,\epsilon^{\mathrm{el}} \\ \delta m_{wS}^{\mathrm{el}} \\ \delta m_{\mathrm{Na}S}^{\mathrm{el}} \end{bmatrix}, \quad \delta\mathbf{s} = 2G\,\mathrm{dev}\,\delta\epsilon^{\mathrm{el}}. \tag{4.4}$$

The incremental bulk modulus B and the coefficients B_k and β_{kl} are defined as follows:

$$B = \frac{\bar{p}}{\kappa}, \quad B_k = B\,\mathrm{Ln}\,\frac{\bar{p}}{\bar{p}_\kappa}\frac{\partial\kappa}{\partial m_{kS}^{\mathrm{el}}}, \quad k = w, \mathrm{Na}, \tag{4.5}$$

and

$$\beta_{kl} = \beta_{lk} = \frac{B_k B_l}{B} - F(\bar{p}, \bar{p}_\kappa)\frac{\partial^2\kappa}{\partial m_{kS}^{\mathrm{el}}\partial m_{lS}^{\mathrm{el}}} + \frac{RT}{m_k^{(M)} m_{kS}^{\mathrm{el}}}\gamma_k I_{kl}, \quad k, l = w, \mathrm{Na}, \tag{4.6}$$

where $F(\bar{p}, \bar{p}_\kappa) = \bar{p}\,\mathrm{Ln}\,\bar{p}/\bar{p}_\kappa - \bar{p}$, $\gamma_w = 1 - x_{wS}^{\mathrm{el}}$ and $\gamma_{\mathrm{Na}} = 1 + x_{\mathrm{NaS}}^{\mathrm{el}}/x_{\mathrm{K}S}^{\mathrm{el}}$.

In (4.3), $\mathrm{tr}\,\epsilon_\kappa^{\mathrm{el}}$ is the value of the elastic volume change when the effective mean-stress varies from the convergence stress $\bar{p}_\kappa$ to a small reference value $\bar{p}_0 = 1$ kPa while the pore fluid is distilled water,

$$\mathrm{tr}\,\epsilon_\kappa^{\mathrm{el}} = -\kappa^{\mathrm{dw}}\,\mathrm{Ln}\,\frac{\bar{p}_\kappa}{\bar{p}_0} \quad \text{with } \kappa^{\mathrm{dw}} = \kappa(x_{kS}^{\mathrm{el,dw}}, k \in S^+ \cup \{w\}). \tag{4.7}$$

The chemical variation of κ is detailed in Appendix A of GLH. On the other hand, the elastic shear modulus G is assumed to be unaffected by chemical effects, so that there is no coupling between shear components and chemical variables.

4.2. Elastic–plastic constitutive equations

With respect to the analyses in LHG and GL, the presence of several cations not only requires to account explicitly for electroneutrality but it also introduces new aspects in the behaviour, since the relative contents of the two cations vary. These aspects have been introduced in the elastic behaviour through the κ-dependence in the molar fractions of the cations. However, experimental data available so far in the literature do not reveal effects on the plastic behaviour typical of the presence of several cations. Therefore, the elastic–plastic model developed in GLH follows the trend of the model for homoionic clays in LHG, to within the important fact that the relative contents of the cations will be kept trace of. The main features of the elastic–plastic behaviour are motivated by the experimental observations of Di Maio and Onorati (1999) on Bisaccia clay.

4.2.1. Mechanical loading

The specimen is in contact with a large reservoir of constant chemical composition and at atmospheric pressure, so that $p_W \sim 0$. The load is continuously varied, sufficiently slowly however in such a way that electro-chemical equilibrium can be established at the end of each load increment, $\bar{\mu}_{wS} = \bar{\mu}_{wW}$ and $\bar{A}_S = \bar{A}_W$. Experiments show that the $e - \mathrm{Ln}\,\bar{p}$ curves are approximately straight and converging to a small void ratio interval. However, the slopes of the loading and unloading curves decrease as the Na-content of the pore water increases. This trend holds whatever this content, that is from zero Na-content (distilled water) to saturated solutions.

4.2.2. Chemical loading: chemical consolidation and swelling

Under constant mechanical conditions, a chemical loading consists in varying the Na- or K-content of the pore water. When the latter increases, the void ratio decreases, and this decrease rate is especially large at small salt content. When the specimen is re-exposed to distilled water, its volume increases. These volume changes are in qualitative agreement with the osmotic effect: increase of salt content leads to an increase of pore water pressure, and this in turn leads to water desorption. Alternatively, one may say that water desorption/absorption occurs to equilibrate the salt contents in pore water and clay pockets. The volume changes depend very much on the loading history: the key phenomenon being that the presence of potassium reduces considerably both elastic and elastic–plastic compliances of clays.

The behaviour qualitatively described above is now given an analytic expression. The superscript pl denotes the plastic contribution to a generalized strain, for example,

$$\epsilon = \epsilon^{\mathrm{el}} + \epsilon^{\mathrm{pl}}, \quad m_{kS} = m_{kS}^{\mathrm{el}} + m_{kS}^{\mathrm{pl}}, \quad k = w, \mathrm{Na}, \mathrm{K}. \tag{4.8}$$

The inequality dissipation (3.1) becomes,

$$\delta D_1 = -\bar{p}\,\mathrm{tr}\,\delta\epsilon^{\mathrm{pl}} + \mathbf{s} : \mathrm{dev}\,\delta\epsilon^{\mathrm{pl}} + \bar{\mu}_{wS}\delta m_{wS}^{\mathrm{pl}} + \bar{A}_S\delta m_{NaS}^{\mathrm{pl}} \geqslant 0. \tag{4.9}$$

If, for simplicity, one restricts the stress dependence to the two first invariants $\bar{p}$ and q, that expression motivates the generalized normality flow rule

$$\operatorname{tr}\delta\epsilon^{\mathrm{pl}} = -\delta\Lambda\frac{\partial g}{\partial\bar{p}}, \quad \operatorname{dev}\delta\epsilon^{\mathrm{pl}} = \delta\Lambda\frac{\partial g}{\partial q}\frac{3}{2}\frac{\mathbf{s}}{q}, \quad \delta m_{wS}^{\mathrm{pl}} = \delta\Lambda\frac{\partial g}{\partial\bar{\mu}_{wS}}, \quad \delta m_{\mathrm{Na}S}^{\mathrm{pl}} = \delta\Lambda\frac{\partial g}{\partial\bar{A}_S}, \tag{4.10}$$

with the generalized potential $g = g(\bar{p}, q, \bar{\mu}_{wS}, \bar{A}_S)$. The yield function f has the same arguments as g plus $\operatorname{tr}\epsilon^{\mathrm{pl}}$ which allows for hardening and softening, for example when the yield function and plastic potential are of the Modified Cam-Clay type, namely

$$f = f(\bar{p}, q, \bar{\mu}_{wS}, \bar{A}_S, \operatorname{tr}\epsilon^{\mathrm{pl}}) = \frac{q^2}{M^2\bar{p}} + \bar{p} - p_c, \tag{4.11}$$

with $M = M(\bar{\mu}_{wS}, \bar{A}_S)$ and $p_c = p_c(\bar{\mu}_{wS}, \bar{A}_S, \operatorname{tr}\epsilon^{\mathrm{pl}})$. The incremental elastic–plastic relations are reported in Appendix B. The major symmetry of the elastic–plastic incremental relations holds iff the flow rule is associative, namely $f = g$. The calibrations of typical interpolation functions for λ and M in terms of $\{\bar{\mu}_{wS}, \bar{A}_S\}$ are provided in Appendix C of GLH together with the hardening/softening rule contained in p_c whose differential

$$(\lambda - \tilde{\kappa})\frac{\delta p_c}{p_c} = -\delta\operatorname{tr}\epsilon^{\mathrm{pl}} + \operatorname{Ln}\frac{\bar{p}_\lambda}{p_c}\delta\lambda - \operatorname{Ln}\frac{\bar{p}_\kappa}{p_c}\delta\tilde{\kappa}, \tag{4.12}$$

appears as a modification of the usual Cam-Clay expression. The dependence $\tilde{\kappa} = \tilde{\kappa}(\bar{\mu}_{wS}, \bar{A}_S)$ is introduced to simplify formally the rate equations.

5. Finite element formulation

5.1. The semi-discrete equations

The field equations to be satisfied are the balance of momentum of the porous medium as a whole, Eq. (2.20), the global balance of mass, Eq. (2.19), the balances of mass of the three ionic species, the two transfer equations (3.4), and a weak enforcement of electroneutrality.

Boundary data can be given in terms of either primary unknowns or in terms of the fluxes that appear in the right-hand sides of the weak forms below. The eight primary unknown fields are interpolated, within the generic element e, in terms of nodal values through a priori distinct shape functions, namely

- the solid displacement $\mathbf{u} = \mathbf{N}_u\mathbf{U}^e$;
- the fluid pressure $p_W = \mathbf{N}_p\mathbf{P}_W^e$;
- the concentrations of ionic species in fluid phase $c_{kW} = \mathbf{N}_c\mathbf{C}_{kW}^e$, $k = \mathrm{Na}, \mathrm{K}, \mathrm{Cl}$;
- the mass-contents of absorbed water and of absorbed sodium $m_{kS} = \mathbf{N}_m\mathbf{M}_{kS}^e$, $k = w, \mathrm{Na}$;
- the electrical potential $\phi_W = \mathbf{N}_\phi\mathbf{\Phi}_W^e$.

Multiplying the eight field equations by the virtual fields $\delta\mathbf{w}$, δp, δc, δm and $\delta\phi$, and integrating by parts over the body V provides the weak form of the problem as:

$$
\begin{aligned}
&\int_V \nabla(\delta\mathbf{w}) : \boldsymbol{\sigma}\,\mathrm{d}V - \int_V \delta\mathbf{w}\cdot(\rho\mathbf{g})\,\mathrm{d}V = \int_{\partial V} \delta\mathbf{w}\cdot\boldsymbol{\sigma}\cdot\hat{\mathbf{n}}\,\mathrm{d}S,\\
&\int_V \delta p\,\mathrm{div}\,\mathbf{v}_S - \nabla(\delta p)\cdot\mathbf{J}_W\,\mathrm{d}V = -\int_{\partial V} \delta p\mathbf{J}_W\cdot\hat{\mathbf{n}}\,\mathrm{d}S,\\
&\int_V \delta c n_W \frac{\delta c_{kW}}{\delta t} + \delta c\sum_{l\in S^{\leftrightarrow}}(I_{kl}-c_{kW})\frac{\delta v_{lS}}{\delta t} + \nabla(\delta c)\cdot\alpha_k\,\mathrm{d}V + \int_V \delta c\mathbf{J}_W\cdot\nabla c_{kW}\,\mathrm{d}V = \int_{\partial V}\delta c\alpha_k\cdot\hat{\mathbf{n}}\,\mathrm{d}S,\\
&\quad k=\mathrm{Na},\mathrm{K},\mathrm{Cl},\\
&\int_V \delta m\left(\frac{1}{T_w}\frac{\delta m_{wS}}{\delta t} - (\bar{\mu}_{wW}-\bar{\mu}_{wS}) - \frac{T_{w\mathrm{Na}}}{T_w}(\bar{A}_W-\bar{A}_S)\right)\mathrm{d}V = 0,\\
&\int_V \delta m\left(\frac{1}{T_{\mathrm{Na}}}\frac{\delta m_{\mathrm{Na}S}}{\delta t} - \frac{T_{\mathrm{Naw}}}{T_{\mathrm{Na}}}(\bar{\mu}_{wW}-\bar{\mu}_{wS}) - (\bar{A}_W-\bar{A}_S)\right)\mathrm{d}V = 0,\\
&\int_V \nabla(\delta\phi)\cdot(-\mathbf{I}_{\mathrm{e}W})\,\mathrm{d}V = -\int_{\partial V}\delta\phi\mathbf{I}_{\mathrm{e}W}\cdot\hat{\mathbf{n}}\,\mathrm{d}S,
\end{aligned}
\tag{5.1}
$$

where

$$
\alpha_k = -\sum_{l\in W}(I_{kl}-c_{kW})\mathbf{J}^d_{lW},\quad k=\mathrm{Na},\mathrm{K},\mathrm{Cl},
\tag{5.2}
$$

and $\hat{\mathbf{n}}$ is the unit outward normal to the boundary ∂V.

In space dimension n_{sd}, the global unknown vector $\mathbb{X}$,

$$
\mathbb{X} = [\,\mathbf{U}\quad \mathbf{P}_W\quad \mathbf{C}_{\mathrm{NaW}}\quad \mathbf{C}_{\mathrm{K}W}\quad \mathbf{C}_{\mathrm{Cl}W}\quad \mathbf{M}_{wS}\quad \mathbf{M}_{\mathrm{Na}S}\quad \boldsymbol{\Phi}_W\,]^{\mathrm{T}},
\tag{5.3}
$$

has maximum nodal length $n_{\mathrm{sd}}+7$. The resulting non-linear first-order semi-discrete equations imply the residual $\mathbb{R}$,

$$
\mathbb{R} = \mathbb{F}^{\mathrm{surf}}(\mathbb{S},\mathbb{X}) - \mathbb{F}^{\mathrm{int+grav}}\left(\mathbf{g},\mathbb{X},\frac{\delta\mathbb{X}}{\delta t}\right) - \mathbb{F}^{\mathrm{adv}}\left(\mathbb{X},\frac{\delta\mathbb{X}}{\delta t}\right) = \mathbb{O},
\tag{5.4}
$$

to vanish. Here $\mathbb{F}^{\mathrm{surf}}$ is the vector of surface loadings denoted collectively $\mathbb{S}$. $\mathbb{F}^{\mathrm{int+grav}}$ is the vector gathering the internal viscous and elastic–plastic forces, as well as the gravity forces appearing in the left-hand-side of (5.1). $\mathbb{F}^{\mathrm{adv}}$ is the sum of element contributions due to SUPG stabilization of advection, see GL for details.

5.2. Time integration

The time integration is performed within an explicit/implicit operator splitting scheme through an Euler scheme, as in GL. At iteration i of time step n, the iterative Newton direction $\Delta\mathbb{V}$ is obtained by insertion of the time-integrator in the residual $\mathbb{R}$, linearizing and setting the result to zero,

$$
\mathbb{C}^*(\Delta\mathbb{V}) = \mathbb{R}^i_{n+1}.
\tag{5.5}
$$

The effective diffusion matrix $\mathbb{C}^*$ is expressed in terms of the diffusion matrix $\mathbb{C}$ and of the stiffness matrix $\mathbb{K}$,

$$
\mathbb{C}^* = \mathbb{C} + \Delta t\mathbb{K}\quad\text{with}\quad \mathbb{C} = \frac{\partial\mathbb{F}_I}{\partial\mathbb{V}}\left(\mathbb{X}^i_{n+1}\right),\quad \mathbb{K} = \frac{\partial\mathbb{F}_I}{\partial\mathbb{X}}\left(\mathbb{X}^i_{n+1}\right),
\tag{5.6}
$$

where $\mathbb{F}_I$ is the sum of implicit operators, namely internal forces and stabilizing advective forces, and it has been recognized that the derivatives of $\mathbb{F}_I$ do not depend on rates.

The element contributions to the block components in the matrices above are given in Appendix C, when the virtual primary unknowns are discretized with the same shape functions as the actual unknowns, advection requiring a special treatment.

The elastic–plastic constitutive equations are integrated at each Gauss point using an extension of the cutting plane algorithm as defined for elastic–plastic solids by Simo and Hughes (1987): this algorithm entails only explicit computations and it iteratively enforces the yield condition within a given strict tolerance.

The global iteration process uses the full Newton-Raphson procedure. The time-step chosen in order to keep the number of equilibrium iterations to a reasonable value was observed to increase as consolidation got established, with a minimum of 0.10 s.

Iterations are stopped when the criteria below involving both residuals and unknowns are satisfied:

- maximum residual force/maximum applied force $= 5\times10^{-4}$;
- maximum correction of solid displacement $= 10^{-4}$ m; of pore pressure $= 5$ Pa;
- maximum correction of ion concentration over its actual value $= 3\times10^{-4}$, of absorbed mass of water $= 3\times10^{-4}$, of absorbed mass of $Na^{+} = 9\times10^{-4}$;
- maximum correction of effective affinity $\bar{A}_W$ (unit: m^2/s^2) $= 0.025$ if $|\bar{A}_W| < 5000$, else $= 5\times10^{-6}|\bar{A}_W|$.

The finite element discretization involves quadratic solid displacements (three nodes per element) while the other seven unknowns vary linearly (two nodes per element). The number of integration points and history points are two, for all stiffness matrices and all residuals. Plastic history is stored at the same two points.

A single mesh has been used for all tests: for the porous stone, it involves 14 elements of length ranging from 0.025 to 0.4 mm. In the upper half sample, 27 elements of length increasing from 0.1 mm close to the porous stone to 0.4 mm at the center. The qualitative accuracy of the results has been checked with a mesh twice finer.

Once the primary variables are known, the dependent variables may be obtained as indicated in Appendix D.

6. Simulations of chemo-mechanical oedometric tests

The model for mass transfer, diffusion, advection and elastic–plastic deformation for heteroionic expansive clays described in the previous sections is now used to simulate oedometric tests on Ponza Clay performed by Di Maio (1996, 1998). Complex paths involving interspersed mechanical and chemical loadings and unloadings have been simulated in GL in the framework of homoionic clays. Here focus is on heteroionic clays and on the effects of the periodic modifications of the chemical composition of the reservoir according to the typical scheme: distilled water—saturated NaCl solution—distilled water—saturated KCl solution—distilled water.

6.1. Material parameters and loading conditions

Initially, the specimen is in contact with distilled water. The initial material state is given in Tables 1 and 2. The material parameters corresponding to Ponza Clay have been defined in LHG and are reported in Tables 3 and 4.

Table 5 shows the parameters defining the transport and transfer properties. The hydraulic conductivity K_h is estimated by equating the numerical and experimental consolidation times in a purely mechanical test bringing, over a linear ramp of 5 sec, the normally consolidated material from 40 to 80 kPa, pore water being kept distilled; the experimental information is provided by Fig. 9 of Di Maio (1996). The value K_{h0} indicated in Table 5 is linked to the void ratio e_0^*.

Table 1
Initial data for Ponza Clay in equilibrium with distilled water and physical constants

Void ratio	$e_0^* = 4.63$
Preconsolidation stress	$p_{c0} = 40$ kPa
Water pressure	$p_W = 0$ kPa
Valence of clay	$\zeta_c = -0.341$
Molar mass of clay	$m_c^{(M)} = 384$ gm
Tortuosity	$\tau = 0.2$

Table 2
Initial repartition of mass-contents (unit: kg/m^3) and of the corresponding molar fractions in the solid phase in equilibrium with distilled water at $\bar{p} = 40$ kPa

Water	$m_{wS} = 79.26$	$x_{wS} = 0.837$
Cation Na^+	$m_{NaS} = 4.485$	$x_{NaS} = 0.037$
Cation K^+	$m_{KS} = 0.847$	$x_{KS} = 0.004$
Anion Cl^-	$m_{ClS} = 0.000$	$x_{ClS} = 0.000$
Clay mineral	$m_{cS} = 244.00$	$x_{cS} = 0.121$

Table 3
Mechanical parameters

κ_{Na}^{dw}	κ_{Na}^{sat}	λ_{Na}^{dw}	λ_{Na}^{sat}	κ_{K}^{dw}	κ_{K}^{sat}	λ_{K}^{dw}	λ_{K}^{sat}
0.081	0.011	0.171	0.101	0.020	0.011	0.110	0.101

Table 4
Mechanical model coefficients

κ_{1Na}	κ_{3Na}	λ_{1Na}	λ_{3Na}	κ_{1K}	κ_{3K}	λ_{1K}	λ_{3K}	K_{eq}	$\bar{p}_\kappa$ (kPa)	$\bar{p}_\lambda$ (kPa)
−0.07	6.0	−0.07	6.0	−0.009	6.0	−0.009	6.0	5.0	1400	2600

Table 5
Hydro-electrical transport, diffusion and physico-chemical transfer parameters

Hydraulic conductivity	$K_{h0} = 0.495 \times 10^{-10}$ m/s
Electro-osmotic conductivity	$k_e = 37.5 n_W \tau \times 10^{-9}$ m/s/V
Effective diffusion coefficients:	$\Longleftrightarrow$ effective ionic mobilities:
$D_{Na}^* = 0.267 \times 10^{-9}$ m^2/s	$u_{Na}^* = 10.397 \times 10^{-9}$ m^2/s/V
$D_{K}^* = 0.387 \times 10^{-9}$ m^2/s	$u_{K}^* = 15.070 \times 10^{-9}$ m^2/s/V
$D_{Cl}^* = 0.403 \times 10^{-9}$ m^2/s	$u_{Cl}^* = 15.694 \times 10^{-9}$ m^2/s/V
Transfer times:	$\Longleftrightarrow$ transfer coefficients:
$\tau_w = 7.40$ s	$T_w = 10^{-3}$ kg s/m^5
$\tau_{Na} = 7.75 \times 10^6$ s	$T_{Na} = 4 \times 10^{-9}$ kg s/m^5

The diffusion coefficients are calibrated by equating the numerical and experimental consolidation times in chemical consolidation tests at constant load and in absence of pore pressure gradient, the experimental reference being the same as above.

No data specific to Ponza Clay are available that would allow a definite determination of the transfer time τ_w. Therefore, in GL, a parameter analysis has been performed to assess its quantitative influence,

starting from the reference value shown in Table 2. As observed in Fig. 1, the transfer time for cations is much larger than that of water. A large tentative value has been adopted.

Some of the parameters listed in Tables 2 and 5 are not independent, e.g. the effective ionic mobilities are deduced from the effective diffusions by the Nernst–Einstein relation. They are nevertheless shown because of their characteristic values.

The oedometer apparatus (height 20 mm, radius 28 mm) presents the advantage of allowing for essentially one-dimensional displacements and flows within the sample. However, a closer look at the flow paths of pore water and salt is necessary, Fig. 3. A discussion is presented in GL and it will not be reiterated here. The height, porosity and diffusion coefficients of porous stone have a very strong influence on the actual chemical loading rate *on* the sample (Table 6): in fact the porous stone damps considerably the external changes of composition of the solution, Fig. 4. In the computations, the porous stone is considered a rigid chemically insensitive porous medium, 4 mm thick. The degrees of freedom associated to the vertical displacements of all nodes within the porous stone are set equal and the degrees of freedom associated to the variations of absorbed masses are fixed and set equal to zero. Due to the symmetry conditions, only the upper half part of the apparatus is meshed.

The boundary conditions at the interface between the reservoir and the porous stone consists in monitoring the following quantities: total traction $\boldsymbol{\sigma}\cdot\mathbf{n}$, fluid pressure p_W, ionic concentrations c_{kW}, $k = \mathrm{Na}$, K, Cl, electrical potential ϕ_W. At the center of the oedometer, the displacement is fixed to zero, the flux of water is zero as well as the diffusive fluxes of ions, and therefore the electric current density.

As mentioned above, the solution in the reservoir is initially distilled water and the sample has been normally consolidated to 40 kPa. The subsequent chemical loading programme simulated involves four stages, Fig. 6:

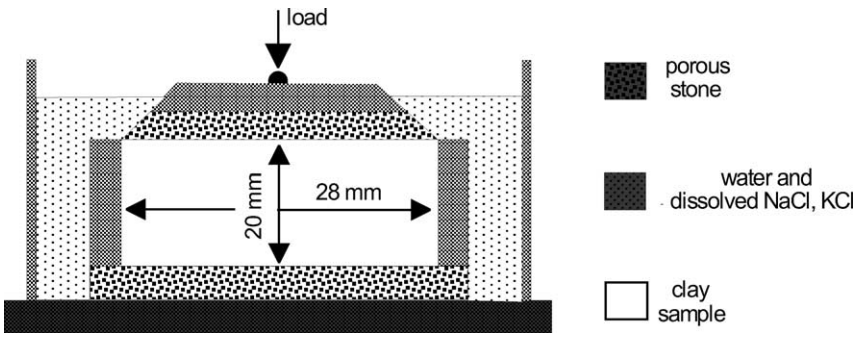

Fig. 3. Schematic of an oedometer test. The sample undergoes instantaneous mechanical loading through a rigid porous stone. Chemical loading is performed by infiltration of a solution of controlled chemical composition through the lateral sides of the porous stone. Note that the solution is kept at atmospheric pressure. A change in composition of the solution reaches the interface porous stone/sample delayed and smoothed out. Moreover, center points receive the change in composition later than peripheral points.

Table 6
Characteristics of the porous stone

Fluid volume fraction	$n_W = 0.4$
Hydraulic conductivity	$K_h = 10^{-4}$ m/s
Electro-osmotic conductivity	$k_e = 1.0 \times 10^{-9}$ m/s/V
Tortuosity	$\tau = 0.6$
Osmotic coefficient	$\omega = 0$

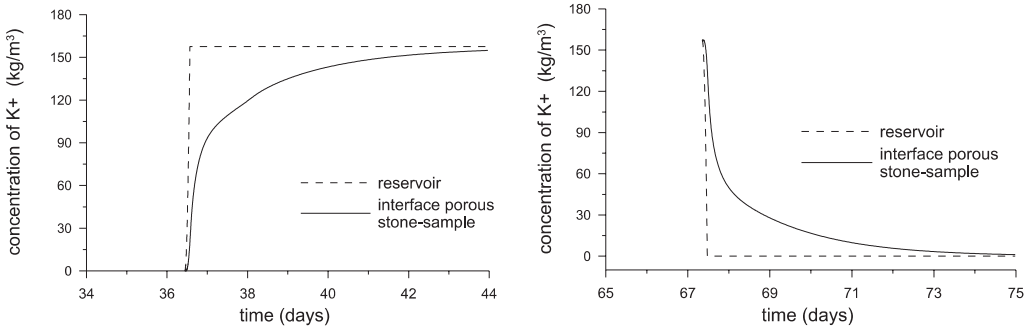

(a) Replacement of distilled water by a KCl-saturated solution

(b) Replacement of KCl-saturated solution by distilled water

Fig. 4. Fast changes of chemical composition of the reservoir are smoothed out by the porous stone. Dashed curve: salt concentration in the reservoir; solid curve: salt concentration at the interface porous stone-sample.

- Stage 1: at time $t = 0$, the NaCl concentration of the reservoir is increased to saturation.
- Stage 2: the NaCl saturated solution of the reservoir is replaced by distilled water.
- Stage 3: the KCl concentration of the reservoir is increased to saturation.
- Stage 4: the KCl saturated solution of the reservoir is replaced by distilled water.

The changes of chemical composition of the reservoir are performed over a parabolic ramp of three hours. Modification of the chemical composition of the reservoir is not attempted before a steady state is reached. This requires of course that chemical consolidation has been established, but it is not sufficient. The fact that the sole consolidation is reached does not imply that the spatial profiles of ionic concentrations are uniform. Each stage, chemical consolidation and swelling, displays, as explained below, four characteristic times, namely

- end of dissipation of negative pore pressures,
- end of dissipation of positive pore pressures,
- end of diffusion of ionic species,
- end of transfer of water and of ionic species.

The evolution in time of the consolidation ratio (stages 1 and 3) and swelling ratio (stages 2 and 4) for purely chemical loading cycles at constant load is compared, in Fig. 5, with a purely mechanical loading cycle, at given reservoir chemistry, in fact distilled water.

The scatter in experimental data shown in Fig. 5 is due to the large range of stress levels involved. The delay in osmotic consolidation is due to the buffer effect of the inert porous stone, across which ions have first to diffuse before reaching the sample. The delay in osmotic swelling is due to both that effect plus the key fact that the mechanical coupling, that is mainly volume expansion, occurs only when the ionic concentration in pore fluid returns to low values, namely less than 1 mol/l. At higher salt concentrations, the mechanical properties change little. Note that consolidation and swelling *ratios* in Fig. 5 are independent, so that possible irreversible effects are concealed by this figure.

Before commenting the physical aspects of the simulations, it is in order to mention some details of the numerical simulations. In particular, water is never completely distilled, ions are always present even in tiny proportions. So the fluid phase that in the text is routinely termed distilled water contains in fact ions with a total molar fraction equal to 10^{-5}. The exact proportions of ions depends on the loading stages. They are implied by the equilibrium of the chemical potentials between the fluid and solid phases, Eq. (3.35) of GLH.

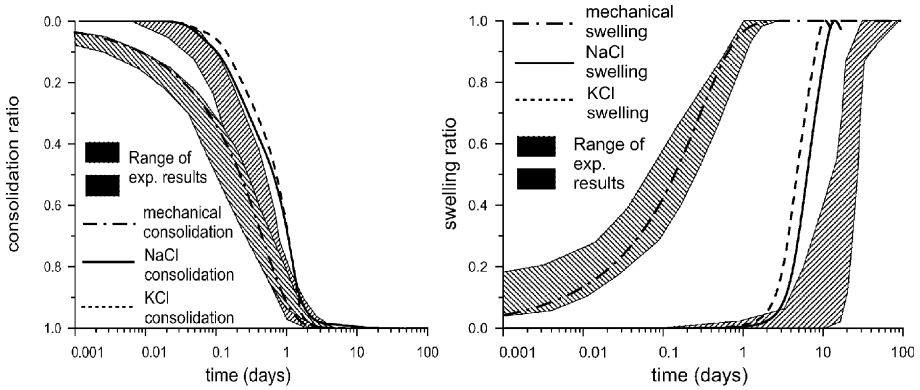

Fig. 5. Osmotic consolidation and swelling ratios resulting from the computations due to replacement of the distilled water of the reservoir by a saturated solution of either NaCl or KCl. Dashed areas: experimental data from Di Maio (1996), her Figs. 9 and 10.

The composition of the solid phase is given as $x_{\mathrm{Na}S}/x_{\mathrm{K}S} = 9, 49, 0.02$ at the beginning of stage 1, and end of stages 2 and 4 respectively. The resulting ratios $x_{\mathrm{Na}W}/x_{\mathrm{K}W}$ in the fluid phase are 45, 245, 0.10 using the equilibrium constant K_{eq} given in Table 4. These values tentatively aim at reproducing the fact that during the experimental process the reservoir is polluted somehow by the electrolyte leaving the sample, the actual concentrations in the reservoir depending on the ratio of its volume and on that of the sample.

6.2. Stages 1 and 3: chemical consolidation

Fig. 4 highlights how the porous stone delays and smooths, at the top of the sample, the rapid change of chemical composition of the reservoir, as already commented on.

During chemical loading, the pore pressure profiles show strong fronts that propagate downwards, Fig. 7. Higher salt concentrations in the upper part of the sample give rise to a negative pore pressure wave (which would induce an upward water flow). In absence of electrical current, the water flux $\mathbf{J}_W$ is equal to $-k_{\mathrm{D}}(\nabla p_W - \omega\nabla\pi)$. Since the pressure is maintained to zero (atmospheric pressure reference) at the top of the sample, negative pressures develop on a downward propagating front, at locations where the osmotic efficiency is large because the salt concentration is small, as far as the low permeability does not allow water to move upwards fast enough. A contrario, a vanishing osmotic efficiency results in a quite different picture, see GL. Correlatively, computations where the osmotic efficiency reaches unity at tiny concentrations displayed much larger negative pore pressures. Interestingly enough, the model based on the a varying tortuosity as in Manassero and Dominijanni (2003) and Malusis and Shackelford (2003) was also observed to give rise to even higher negative pore pressures, even with the osmotic efficiency (3.11): this is due to the fact that the ionic species diffuse initially very slowly so that ω remains large for a while, and the product $\omega\nabla\pi$ turns out to be larger, in early times, than in a constant tortuosity analysis.

As the salt concentration increases, the osmotic efficiency quickly decreases and mechanical coupling at low ionic concentrations induces a volume decrease: both phenomena contribute to bring pore pressures from negative to positive values, except at the top of the sample since the reservoir is maintained at atmospheric pressure. Further increase of salt concentrations does not drive pore pressures any longer. After about three days, they have dissipated and the vertical settlement stabilizes, Figs. 6 and 7.

Ionic diffusion, as controlled by the effective diffusion coefficients, and affected adversely by advection, is slower than the propagation of pore pressures, and a uniform profile requires more than ten days,

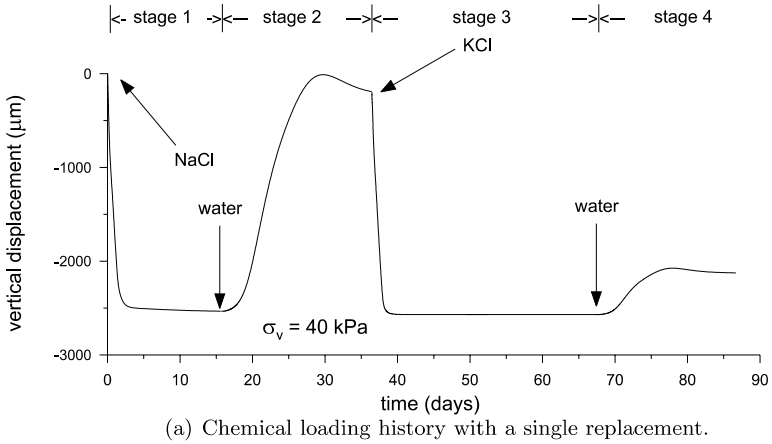

(a) Chemical loading history with a single replacement.

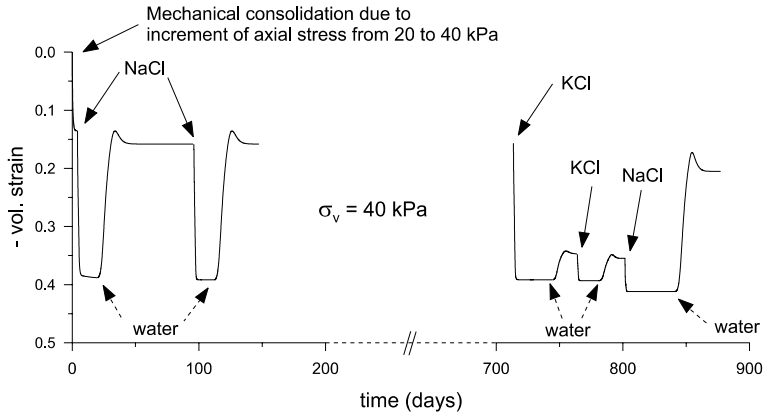

(b) More complex chemical loading histories.

Fig. 6. Evolution of the settlement of the oedometer during changes of the chemical composition of the reservoir at constant vertical stress. These finite element computations compare quite well with the experiments, Fig. 1. (a) Ions K^+ stiffens the material much more than ions Na^+. (b) The effect is essentially reversible. The actual evolution of the vertical settlement depends on the time at which the chemistry of the reservoir is modified. After KCl loading, the reservoir is refreshed 30 days later: the resulting swelling is larger than at the next cycle. This is because all the cations sodium have not been expulsed yet from the interlayers. The volume change upon the last swelling is smaller than in the first swellings due to refreshment of the NaCl saturated solution because there are now some residual cations potassium in the clay platelets.

Figs. 8–10(a) and (c): in fact, completely homogeneous ionic profiles require a much longer period, about 50–60 days.

Water desorption, due to mechanical coupling, shows virtually the same profile since the mass transfer is quasi-instantaneous. Note that ionic concentrations and desorbed masses show diffusive profiles in agreement with the small value of the (global) Péclet numbers $|\mathbf{v}_k^{\mathrm{adv}}|L/D_k^*$, defined by the advective velocities $\mathbf{v}_k^{\mathrm{adv}}$, Eq. (E.2), the half-height of the sample $L = 10$ mm, and the effective diffusion coefficients D_k^*, associated to the three ionic species $k = \mathrm{Na}, \mathrm{K}, \mathrm{Cl}$.

Once positive pore pressures have dissipated, the strain and vertical displacement stabilize even if the salt concentration has not reached a steady state, compare Figs. 6 and 8. Indeed, at salt concentrations larger

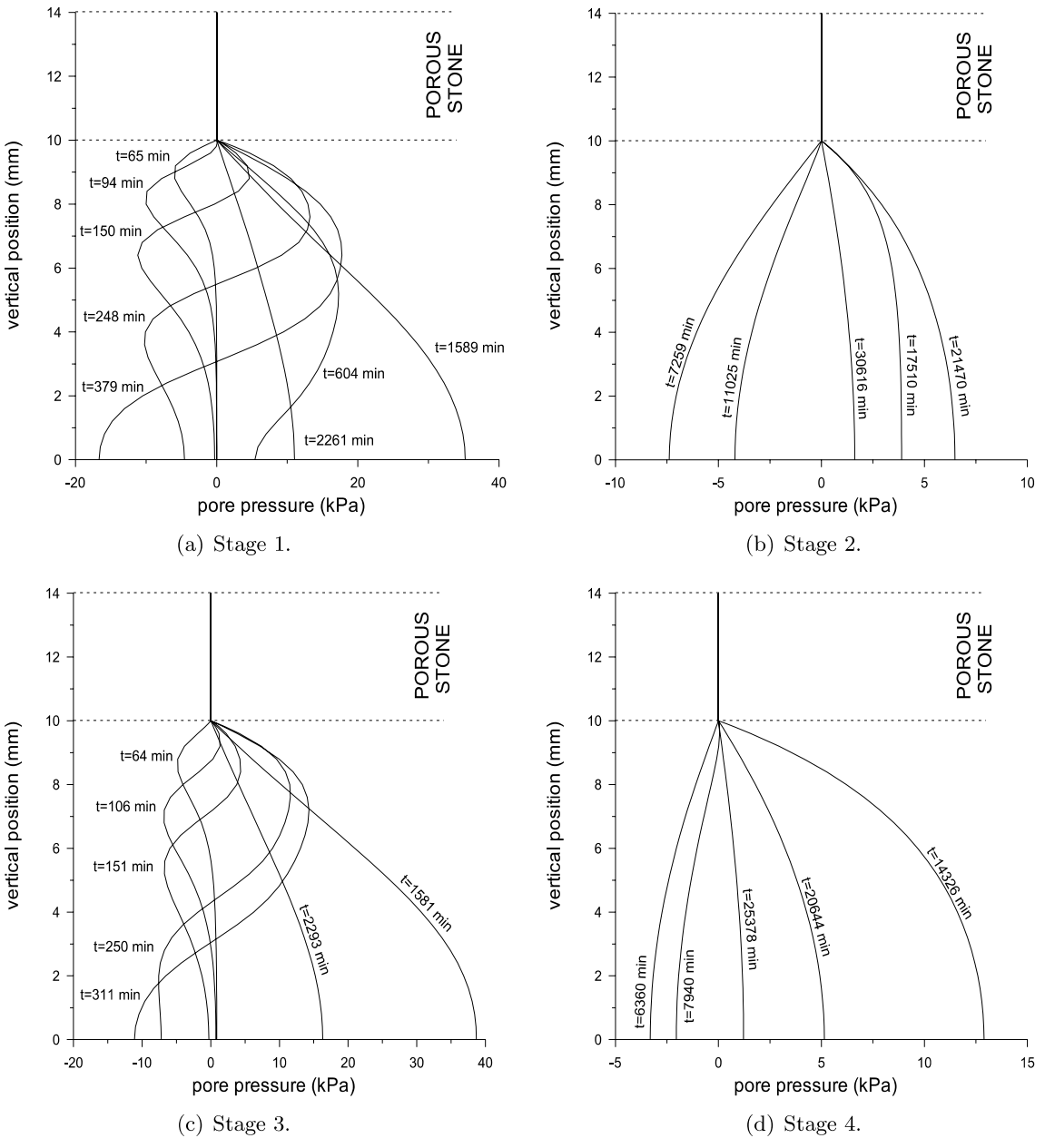

(a) Stage 1. (b) Stage 2.

(c) Stage 3. (d) Stage 4.

Fig. 7. Time and space evolution of the pore pressure in fluid phase during the four loading stages (1 day = 1440 min). In stages 1 and 3 where ionic concentration is increased in the reservoir, osmotic efficiency initially induces negative pore pressures at the center of the oedometer (zero vertical position). As salt diffuses downwards, the osmotic efficiency decreases, and chemical couplings develops, and both phenomena induce pore pressure increase. In stages 2 and 4, where the salt concentration is decreased in the reservoir, osmotic efficiency implies, at intermediate times, increase of pore pressure because the ionic concentration gradient is opposite with respect to stages 1 and 3.

than 1 mol/l, the chemo-mechanical coupling is quite low: the mechanical parameters are quasi independent of the chemical content, Fig. 8 of LHG.

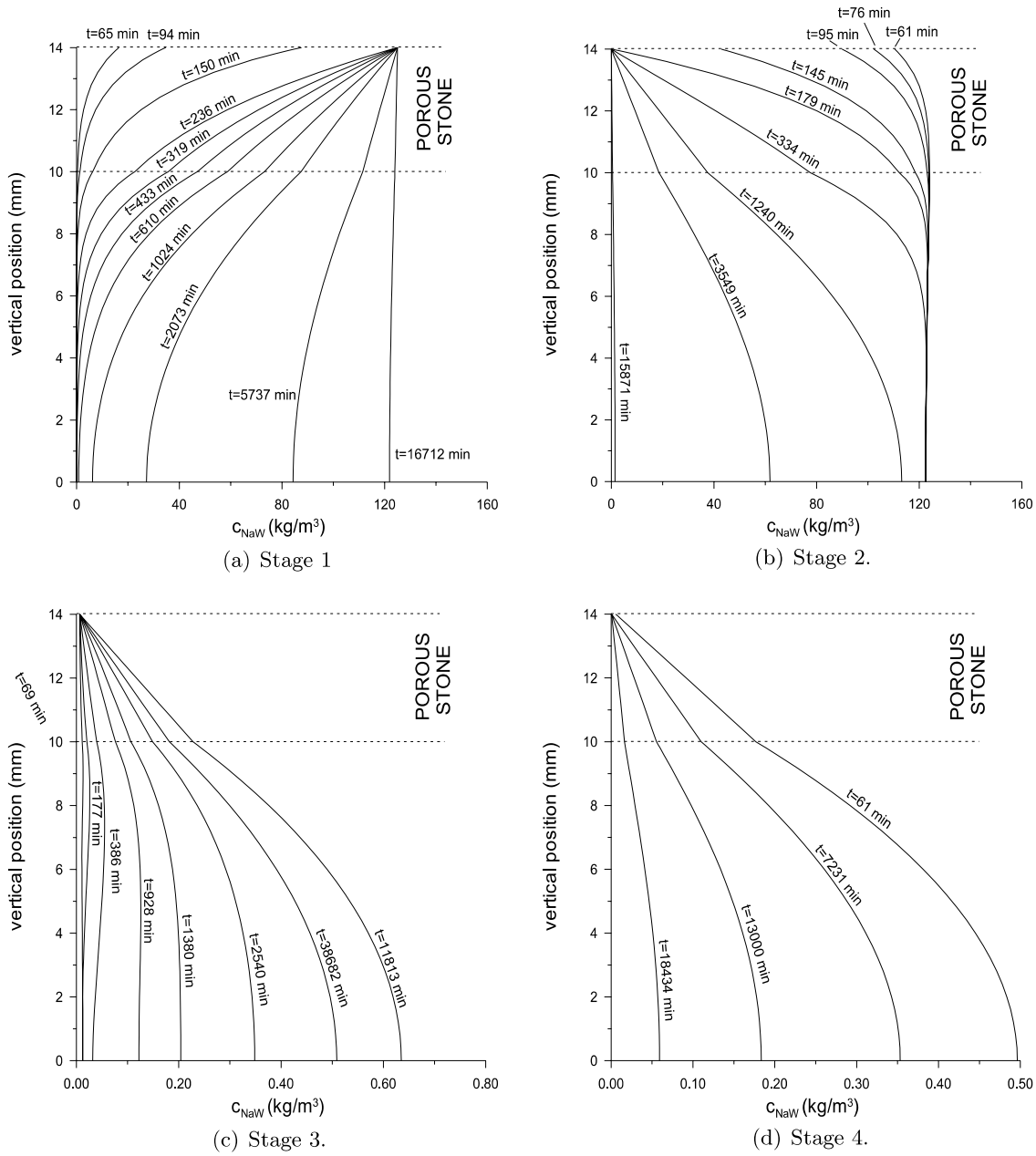

Fig. 8. Time and space evolution of the concentration of ions Na^+ in fluid phase during the four loading stages. Ionic concentration is slower to reach a steady state than pore pressure and settlement. During stages 3 and 4, a few cations Na^+ are present in pore water due to desorption from the solid phase, and not to an incoming flux from the reservoir.

While the above comments pertain essentially to the stage 1 where the reservoir is saturated with NaCl, they apply qualitatively as well for stage 3 where the reservoir is saturated with KCl. The main difference between the two stages is due to the fact that the diffusion of K^+ is faster than that of Na^+, and this speeds somehow the trend to steady state.

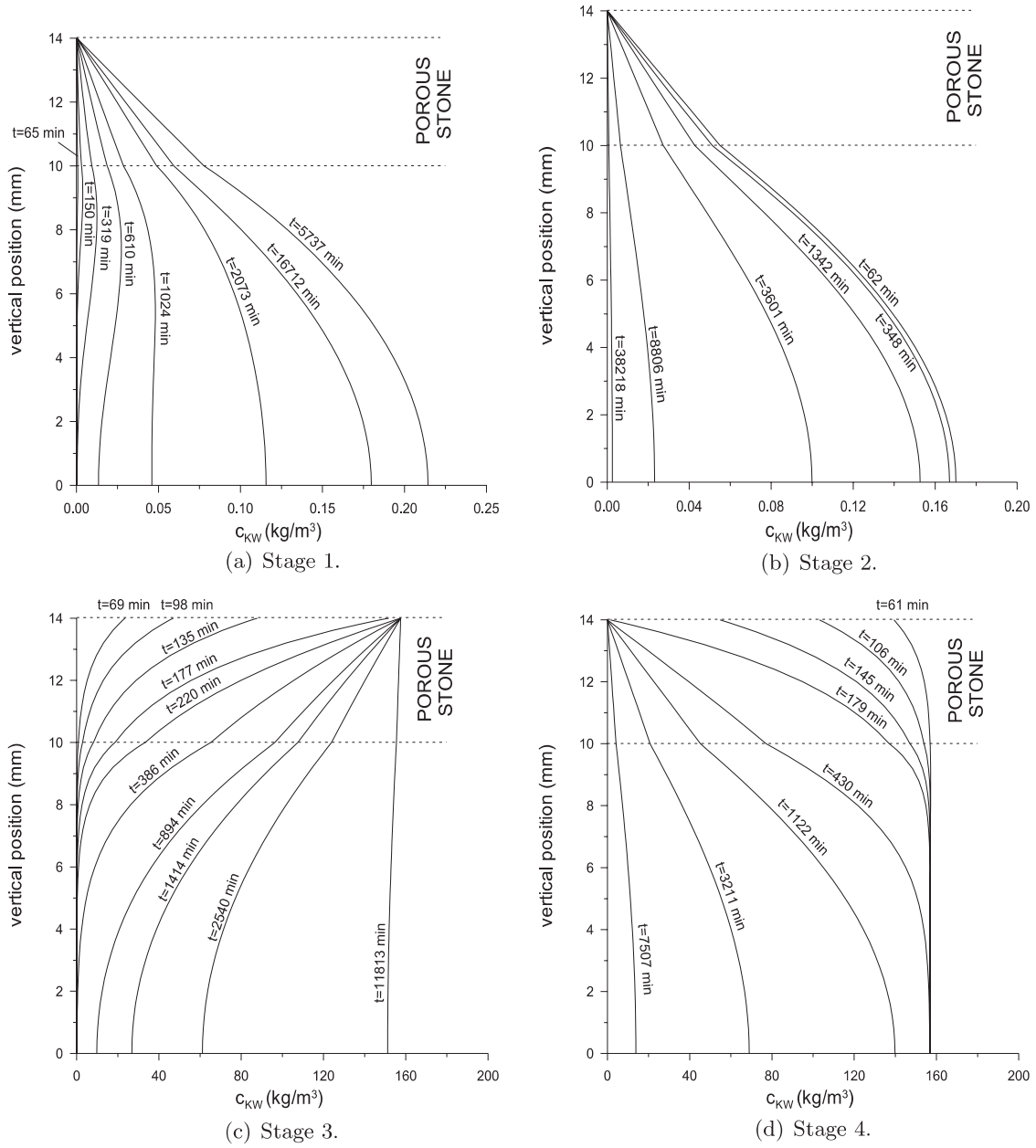

Fig. 9. Time and space evolution of the concentration of ions K^+ in fluid phase during the four loading stages. During stages 1 and 2, a few cations K^+ are present in pore water due to desorption from the solid phase.

6.3. Stages 2 and 4: swelling

As a steady state is approached at the ends of stages 1 and 3, the chemical composition of the reservoir is changed by replacing the saturated solution by distilled water. Times used in each stage refers to the time at which the reservoir chemistry is changed.

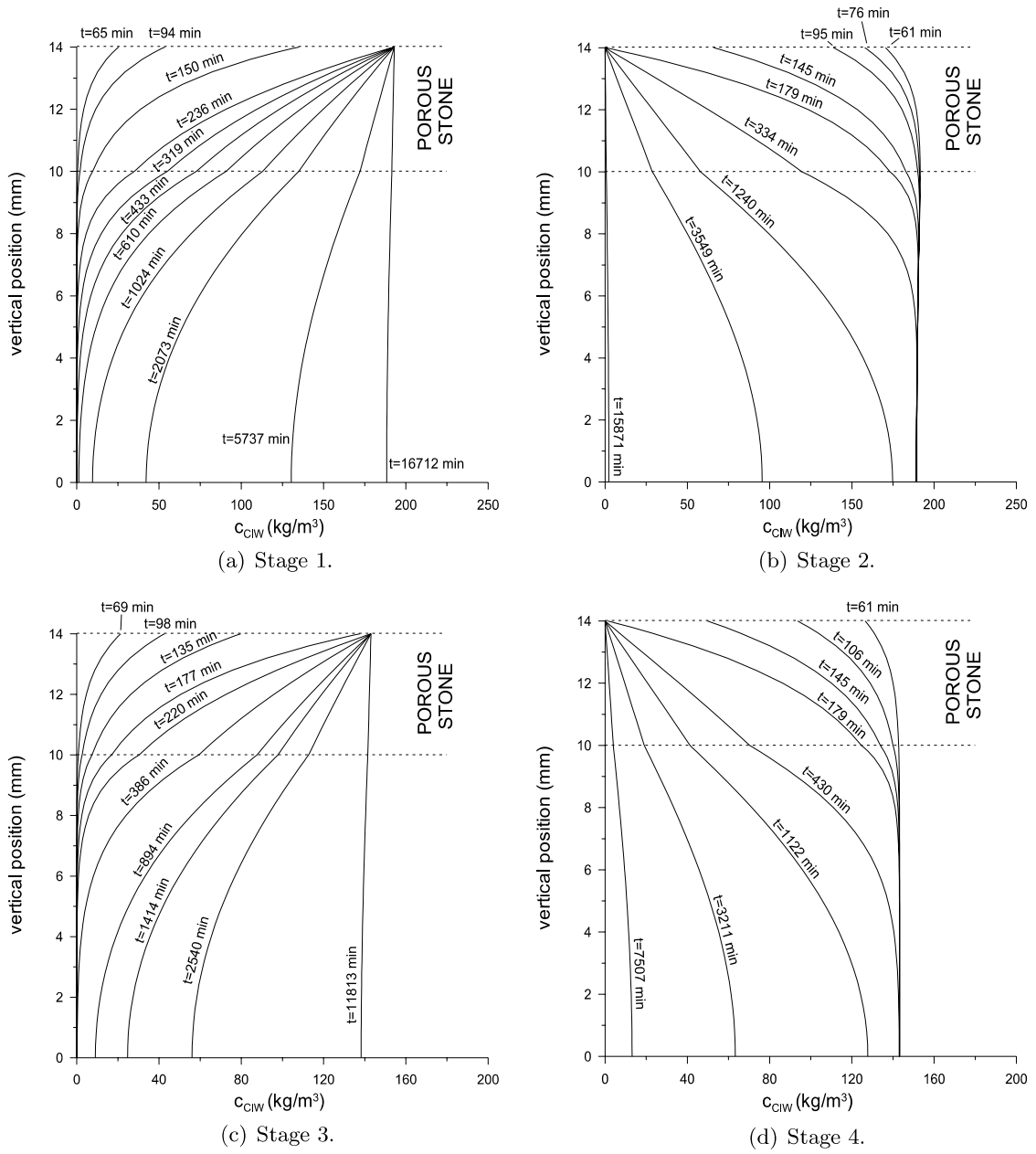

Fig. 10. Time and space evolution of the concentration of ion Cl^- in fluid phase during the four loading stages.

The ionic concentration decreases, Figs. 8–10(b) and (d), and simultaneously the mass of absorbed water increases, Fig. 11. Because practically all cations potassium which were initially in the solid phase have been desorbed during stage 1, in stage 2 cations sodium can not enter neither leave the solid phase due to electroneutrality, Fig. 12(b). Chemo-mechanical coupling implies absorption to induce volume increase, which in turn induces negative pore pressures as the low permeability does not allow for a fast downward

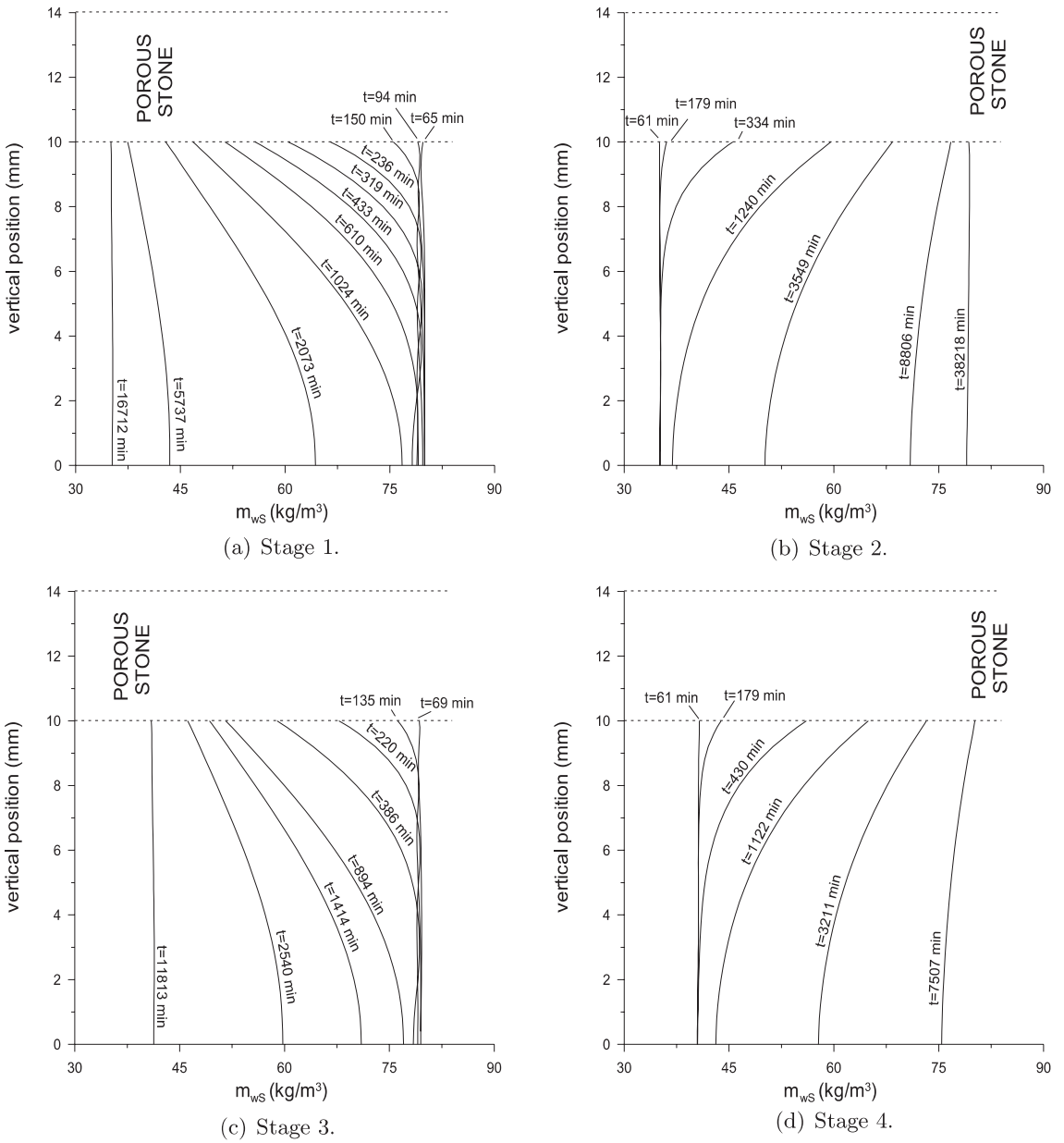

Fig. 11. Time and space evolution of the mass of water in solid phase during the four loading stages. Water desorbs as cation concentration increases, and conversely, essentially in agreement with the osmotic effect.

flow of water, Fig. 7(b) and (d). Notice however that the values of negative pore pressures are not high: this is because the chemo-mechanical coupling, and the trend to swelling, is important only for moderate to small ionic concentrations, as already pointed out.

Negative pore pressures have dissipated after about 8 days, while positive pore pressures develop until day 15. Indeed, the mechanism beyond this pore pressure increase is osmotic efficiency, as the salt gradient is opposite with respect to chemical consolidation. The effective stress is then reduced, due to equilibrium.

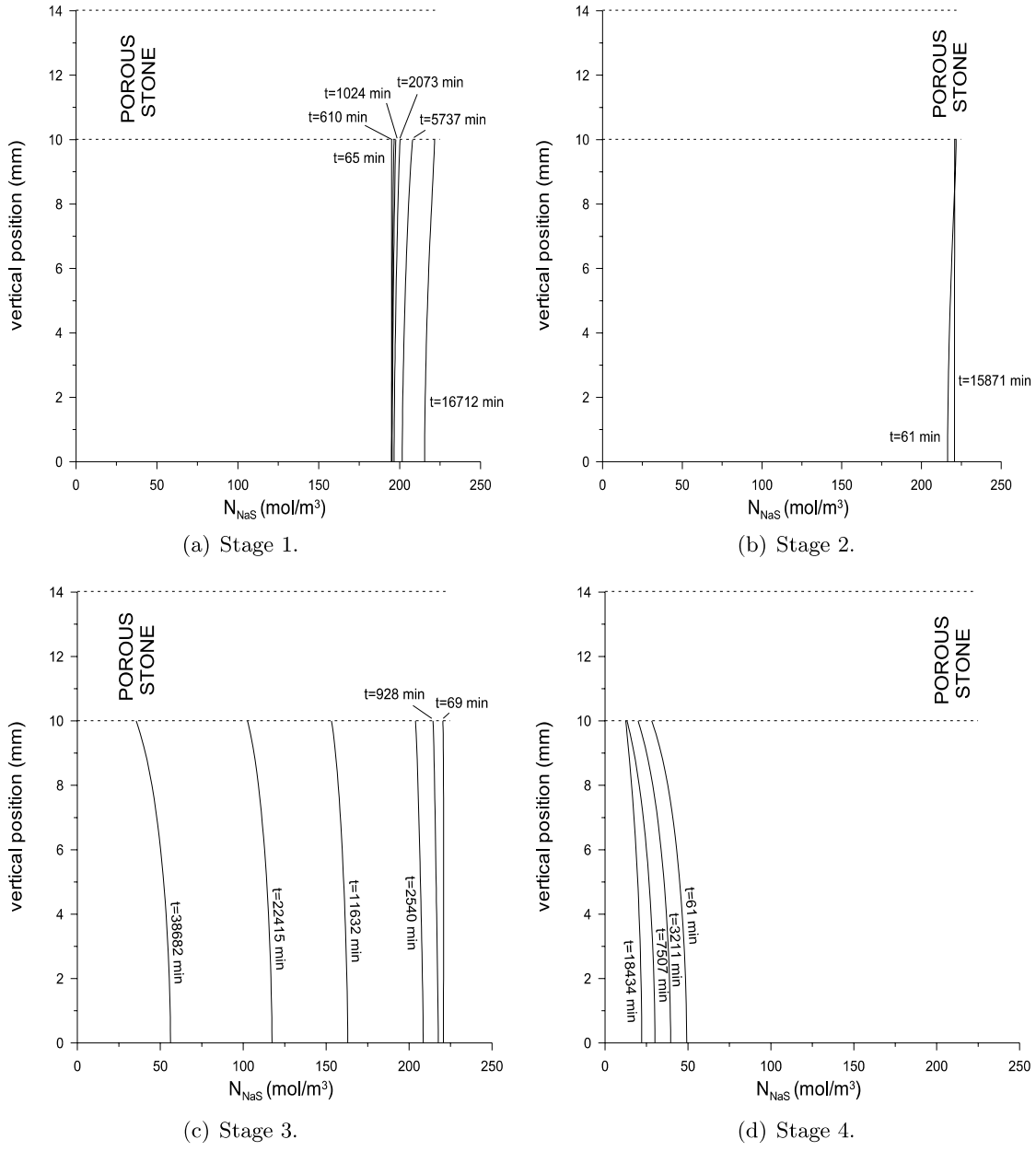

Fig. 12. Time and space evolution of the number of moles of cations Na^+ in solid phase during the four loading stages. Practically all cations potassium which were initially in the solid phase have been desorbed during stage 1, and thus electroneutrality has induced cations sodium to replace them. In stage 2, electroneutrality further prevents cations sodium, which are then the only cations in the solid phase, from being desorbed or absorbed, Fig. 12(b). In stage 3, cations K^+ replace cations Na^+ in the solid phase.

An approximative homogeneous profile of salt concentration is reached in about ten days like for consolidation. For both consolidation and swelling, salt diffusion and water flow occur in opposite directions, so that advection, even if it is small, delays the establishment of a steady state. However, for

consolidation, the chemo-mechanical coupling, which was desorbing water, occurred early during consolidation and the later period was controlled exclusively by salt diffusion. This is no longer the case now, as in fact chemo-mechanical coupling occurs at later times, and so downward flow of absorbed water is in competition with upward flow of salt all along the process. Once again, it should be remembered that the chemo-mechanical coupling is particularly strong at low salt concentration.

The slight final overshoot of the settlement, Fig. 6, is to be linked to the final dissipation of positive pore pressures, and consequent increase of effective stress: this effect is not observed in experiments and might be an artefact of the one-dimensional idealization.

The above comments pertain essentially to the swelling stage 2. Swelling stage 4 differs qualitatively, because the introduction of ions K^+ in the solid phase has ejected ions Na^+ present initially, so that the elastic and plastic compliances at the end of stage 3 are much smaller. Thus swelling results to be much smaller in stage 4.

During the whole chemical loading process, the total vertical stress is equal to 40 kPa and constant (gravity is neglected). Since the pore pressure takes negative and positive values, the effective stress $\bar{p}$ will vary as well. When the pore pressure is negative, the effective stress is larger than 40 kPa and plasticity occurs with strain-hardening. Subsequent chemical loading accompanied with increasing pore pressures, and decreasing effective stress, occurs initially elastically. Later, due to chemical softening, the preconsolidation stress decreases, while the positive pore pressures dissipate, and the effective stress increases again towards 40 kPa. Starting from the porous stone interface, a plastic zone where $p_c = \bar{p}$, with p_c increasing due to strain-hardening, penetrates the sample downwards. At the end of the chemical consolidation, the preconsolidation stress p_c and the effective stress are equal and uniform almost all along the sample, Fig. 13(a).

Upon swelling, chemical preconsolidation develops as described in LHG, their Fig. 5c. In subsequent stages, the negative pore pressures are smaller than in stage 1, so that the effective stress will not pass its previous maximum value, at any point, and plasticity does not develop any longer, Fig. 13. In fact there is not much plasticity even in stages 1 and 2, see Fig. 6. This is in agreement with the data of Di Maio (1996) which indicate that, during chemical loading cycles, plasticity develops at higher stresses only. Even if the mechanical parameters satisfy the relations (5.11) of GLH, the model shows chemical effects on the preconsolidation stress during chemical loading because $\bar{p}_\kappa \neq \bar{p}_\lambda$, Table 3, and these effects are able to imply here chemical preconsolidation, Fig. 13(b)–(d).

As a final remark, let us point out that chemical loading and mechanical loading address different targets. While chemical loading implies significant changes of the amount of absorbed water, Fig. 11, mechanical compression has a much smaller impact on mass exchanges as shown in Fig. 14. In fact, mechanical compression affects mainly pore water.

7. Conclusions

This study is to be understood as a piece of a general framework to both model constitutive behaviour and simulate field problems where electro-chemo-mechanical couplings can not be neglected. It capitalizes upon a previous, formally similar, study for homoionic clays where electrical effects could be disregarded. To the elastic–plastic coupled constitutive equations developed in GLH have been added here equations for diffusion of salt and water, and electrical flow through the porous skeleton as well as mass transfer equations describing the key physical phenomenon of absorption/desorption. The influence of this phenomenon on the mechanical properties is considerable, and the resulting swelling/chemical consolidation poses tremendous problems in the maintenance and stability of geotechnical structures.

Care has been taken to embody the development of these complex aspects in a clear mathematical structure that is nevertheless versatile enough to incorporate necessary refinements.

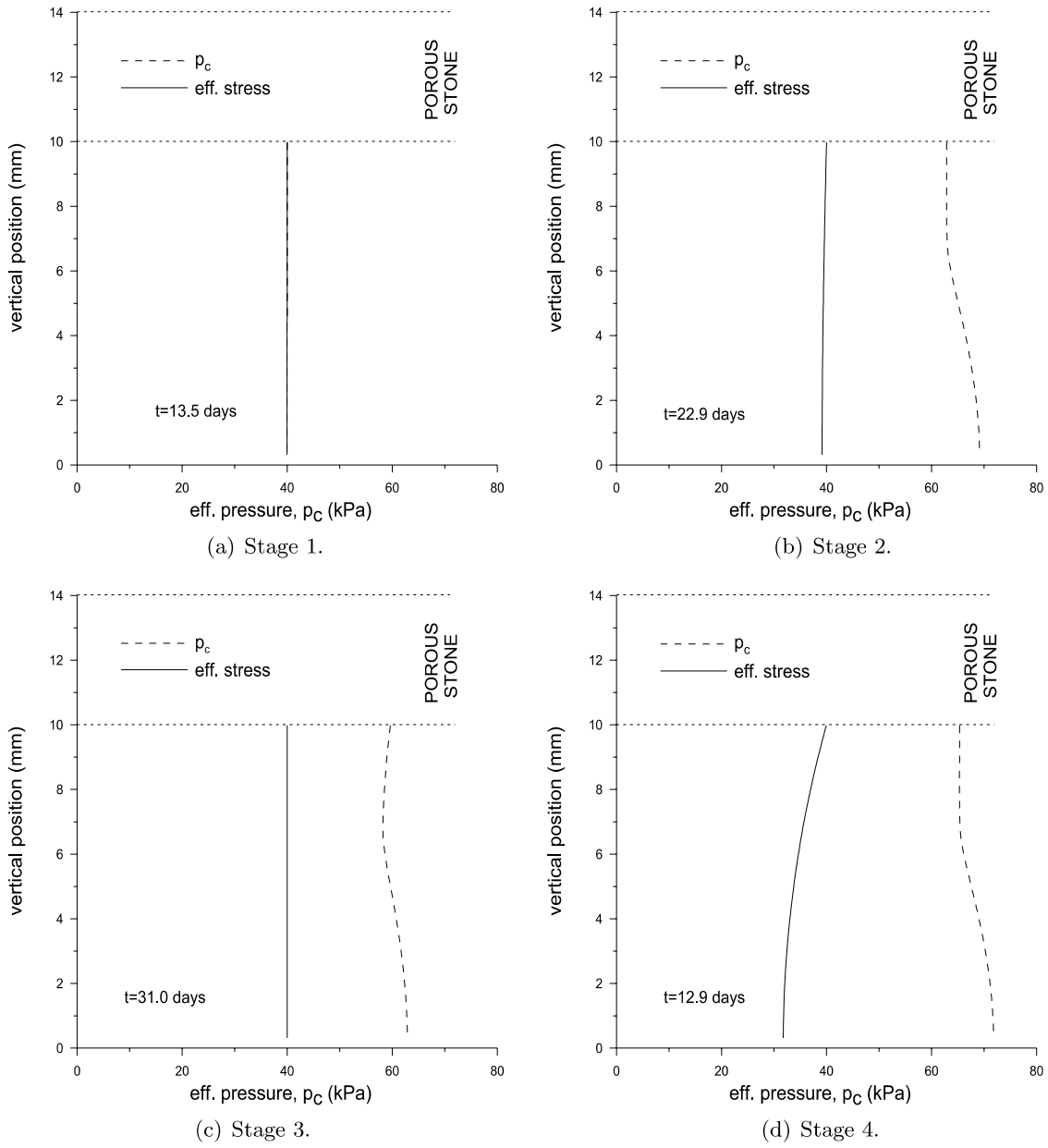

(a) Stage 1. (b) Stage 2.

(c) Stage 3. (d) Stage 4.

Fig. 13. Time and space evolution of the preconsolidation stress p_c during the four loading stages. Chemical influence on p_c implies preconsolidation after stage 1. Time refers to the beginning of each of the four stages.

In GL, attention has been drawned to the interpretation of experimental data, where pointwise homogeneity at steady state within the whole sample might be very difficult to achieve. The present simulations have reiterated the importance of a careful control of all the details of the experimental setup, and of the loading history and loading rates. Too fast loading rates might induce inhomogeneities in the samples and invalidate a pointwise interpretation of steady states.

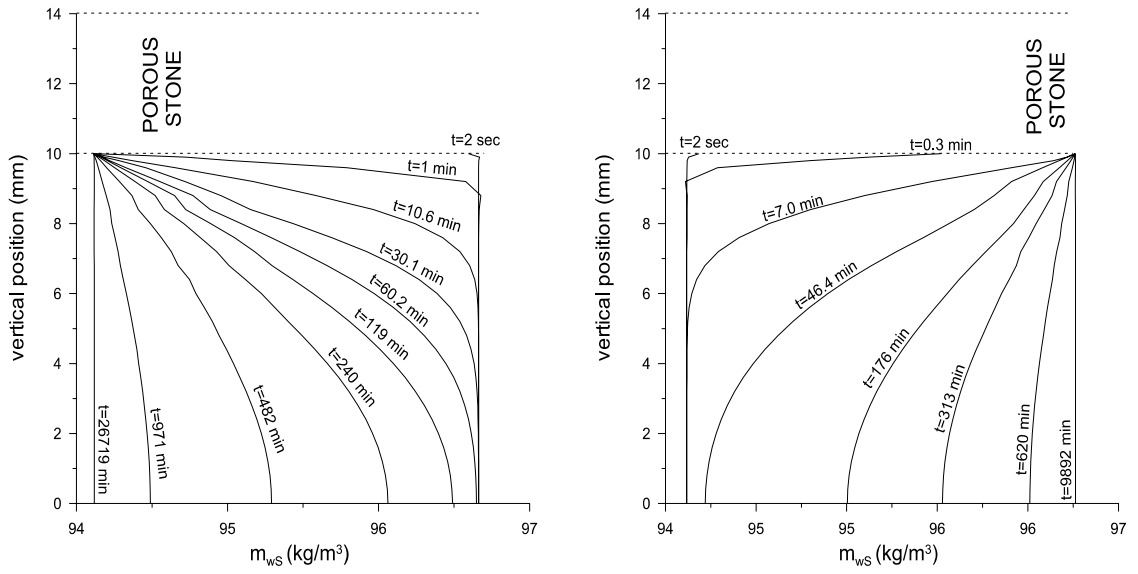

(a) Stage 1. (b) Stage 2.

Fig. 14. Time and space evolution of the mass of absorbed water during the mechanical consolidation and swelling. As expected, absorption/desorption of water is much smaller than during chemical consolidation/swelling, Fig. 11(a) and (b).

Extension of the present analysis is necessary in order to account for the effect of pH. In fact, while pH changes the electrical charge of clay platelets, the present analysis has assumed that quantity to maintain a fixed value.

Appendix A. The electrical current density $\mathbf{I}_{eW}$ is divergence free

Using the decomposition of the change of mass of a species in the fluid phase into a reactive and a diffusive part (2.16), we have

$$F\frac{\zeta_k}{m_k^{(M)}}\frac{\delta}{\delta t}(m_{kW}+m_{kS})+\operatorname{div}\left(F\frac{\zeta_k}{v_k^{(M)}}\mathbf{J}_{kW}\right)=0. \tag{A.1}$$

Summation over W, with the definitions (2.6) for the current densities I_{eS} and I_{eW}, and $(2.15)_1$ of $\mathbf{I}_{eW}$, yields

$$\frac{\delta}{\delta t}\frac{V_0}{V}(I_{eS}+I_{eW})+\operatorname{div}\mathbf{I}_{eW}=0. \tag{A.2}$$

Electroneutrality of the fluid phase implies $\mathbf{I}_{eW}$ defined by (2.15) to be the electrical current density (2.14). Electroneutrality of both solid and fluid phases, i.e. $I_{eS}=0$, $I_{eW}=0$, yields the result (2.18), which thus can be viewed as the divergence of the electrical current density (2.14).

Appendix B. Elastic–plastic stiffness

The incremental elastic–plastic relations can be cast in the following matrix form:

$$\begin{bmatrix} -\delta\bar{p} \\ \delta q \\ \delta\bar{\mu}_{wS} \\ \delta\bar{A}_S \end{bmatrix} = \begin{bmatrix} B^{\mathrm{ep}}_{\bar{p}\bar{p}} & B^{\mathrm{ep}}_{\bar{p}q} & B^{\mathrm{ep}}_{\bar{p}w} & B^{\mathrm{ep}}_{\bar{p}\mathrm{Na}} \\ B^{\mathrm{ep}}_{q\bar{p}} & B^{\mathrm{ep}}_{qq} & B^{\mathrm{ep}}_{qw} & B^{\mathrm{ep}}_{q\mathrm{Na}} \\ B^{\mathrm{ep}}_{w\bar{p}} & B^{\mathrm{ep}}_{wq} & B^{\mathrm{ep}}_{ww} & B^{\mathrm{ep}}_{w\mathrm{Na}} \\ B^{\mathrm{ep}}_{\mathrm{Na}\bar{p}} & B^{\mathrm{ep}}_{\mathrm{Na}q} & B^{\mathrm{ep}}_{\mathrm{Na}w} & B^{\mathrm{ep}}_{\mathrm{NaNa}} \end{bmatrix} \begin{bmatrix} \delta\,\mathrm{tr}\,\epsilon \\ \delta\epsilon_q \\ \delta m_{wS} \\ \delta m_{\mathrm{Na}S} \end{bmatrix}. \tag{B.1}$$

The incremental moduli B^{ep}_{kl} classically differ from their elastic counterparts B_{kl} by a dyadic product, namely:

$$B^{ep}_{kl} = B_{kl} - \frac{1}{H} g_k f_l, \quad k, l \in \{\bar{p}, q, w, \mathrm{Na}\}. \tag{B.2}$$

The coefficients f_k, g_k, $k \in \{\bar{p}, q, w, \mathrm{Na}\}$ entering the elastic–plastic stiffness (B.1) are obtained by the consistency condition $\delta f = 0$:

$$f_k = -B_{k\bar{p}} \frac{\partial f}{\partial \bar{p}} + B_{kw} \frac{\partial f}{\partial \bar{\mu}_{wS}} + B_{k\mathrm{Na}} \frac{\partial f}{\partial \bar{A}_S}; \quad k = \bar{p}, w, \mathrm{Na}, \quad f_q = 3G \frac{\partial f}{\partial q}. \tag{B.3}$$

Similar definitions hold for the g_k's. The elastic coefficients used in the above formulas are read off the elastic constitutive equations:

$$B_{\bar{p}\bar{p}} = B; \quad B_{\bar{p}k} = B_{k\bar{p}} = B_k, \quad k = w, \mathrm{Na}; \quad B_{kl} = \beta_{kl}, \quad k, l = w, \mathrm{Na}; \quad B_{qk} = B_{kq} = 3GI_{kq}, \quad k = \bar{p}, q, w, \mathrm{Na}. \tag{B.4}$$

The plastic modulus H is assumed to take only strictly positive values,

$$H = h - \frac{\partial f}{\partial \bar{p}} g_{\bar{p}} + \frac{\partial f}{\partial q} g_q + \frac{\partial f}{\partial \bar{\mu}_{wS}} g_w + \frac{\partial f}{\partial \bar{A}_S} g_{\mathrm{Na}}, \tag{B.5}$$

while the hardening modulus h will be positive for hardening, and negative for softening,

$$h = \frac{p_c}{\lambda - \kappa} \frac{\partial g}{\partial \bar{p}}. \tag{B.6}$$

For the Modified Cam-Clay model (4.11), the following derivatives are needed,

$$\frac{\partial f}{\partial \bar{p}} = 1 - \frac{1}{M^2} \frac{q^2}{\bar{p}^2}, \quad \frac{\partial f}{\partial q} = \frac{2}{M^2} \frac{q}{\bar{p}}, \quad \frac{\partial f}{\partial Y} = -\frac{2}{M^3} \frac{q^2}{\bar{p}} \frac{\partial M}{\partial Y} - \frac{\partial p_c}{\partial Y}, \quad Y = \bar{\mu}_{wS}, \bar{A}_S, \tag{B.7}$$

where

$$\frac{\partial p_c}{\partial Y} = \left(\mathrm{Ln} \frac{\bar{p}_\lambda}{p_c} \frac{\partial \lambda}{\partial Y} - \mathrm{Ln} \frac{\bar{p}_\kappa}{p_c} \frac{\partial \tilde{\kappa}}{\partial Y} \right) \frac{p_c}{\lambda - \tilde{\kappa}}. \tag{B.8}$$

In component form, the effective constitutive stiffness obtained from Sections 4.1 and 4.2, for an elastic behaviour and an elastic–plastic behaviour respectively, has the following block structure,

$$\mathbf{D} = \left[\begin{array}{c|cc} \mathbf{D}_{uu} & \mathbf{D}_{uw} & \mathbf{D}_{u\mathrm{Na}} \\ \hline \mathbf{D}_{wu} & D_{ww} & D_{w\mathrm{Na}} \\ \mathbf{D}_{\mathrm{Na}u} & D_{\mathrm{Na}w} & D_{\mathrm{NaNa}} \end{array}\right]$$

$$= \left[\begin{array}{c|cc} \mathbb{E} - \frac{1}{H}\mathbf{F}_g \otimes \mathbf{F}_f & B_w\,\mathbf{I} - \frac{1}{H}\mathbf{F}_g\, f_w & B_{\mathrm{Na}}\,\mathbf{I} - \frac{1}{H}\mathbf{F}_g\, f_{\mathrm{Na}} \\ \hline B_w\,\mathbf{I} - \frac{1}{H} g_w\,\mathbf{F}_f & \beta_{ww} - \frac{1}{H}\, g_w\, f_w & \beta_{w\mathrm{Na}} - \frac{1}{H}\, g_w\, f_{\mathrm{Na}} \\ B_{\mathrm{Na}}\,\mathbf{I} - \frac{1}{H} g_{\mathrm{Na}}\,\mathbf{F}_f & \beta_{\mathrm{Na}w} - \frac{1}{H}\, g_{\mathrm{Na}}\, f_w & \beta_{\mathrm{NaNa}} - \frac{1}{H}\, g_{\mathrm{Na}}\, f_{\mathrm{Na}} \end{array}\right]. \tag{B.9}$$

If the yield function depends on stress through $\bar{p}$ and q only, then

$$\mathbf{F}_f = \frac{\partial f}{\partial \bar{\boldsymbol{\sigma}}} : \mathrm{E} + B_w \frac{\partial f}{\partial \bar{\mu}_{wS}}\mathbf{I} + B_{\mathrm{Na}} \frac{\partial f}{\partial \bar{A}_S}\mathbf{I} = f_{\bar{p}}\mathbf{I} + f_q \frac{\mathbf{s}}{q}, \tag{B.10}$$

and similar definitions for the quantities associated to the plastic potential g. E is the tangent elastic stiffness, that is

$$E : \delta\epsilon = B \operatorname{tr} \delta\epsilon \mathbf{I} + 2G \operatorname{dev} \epsilon. \tag{B.11}$$

In matrix form with the Voigt convention, the incremental elastic relations write,

$$\left[\begin{array}{c} \delta\overline{\sigma}_{11} \\ \delta\overline{\sigma}_{22} \\ \delta\overline{\sigma}_{33} \\ \delta\overline{\sigma}_{12} \\ \delta\overline{\sigma}_{23} \\ \delta\overline{\sigma}_{13} \\ \hline \delta\overline{\mu}_{wS} \\ \delta\overline{A}_S \end{array}\right] = \left[\begin{array}{cccccc|cc} B+\frac{4}{3}G & B-\frac{2}{3}G & B-\frac{2}{3}G & 0 & 0 & 0 & B_w & B_{\mathrm{Na}} \\ B-\frac{2}{3}G & B+\frac{4}{3}G & B-\frac{2}{3}G & 0 & 0 & 0 & B_w & B_{\mathrm{Na}} \\ B-\frac{2}{3}G & B-\frac{2}{3}G & B+\frac{4}{3}G & 0 & 0 & 0 & B_w & B_{\mathrm{Na}} \\ 0 & 0 & 0 & G & 0 & 0 & 0 & 0 \\ 0 & 0 & 0 & 0 & G & 0 & 0 & 0 \\ 0 & 0 & 0 & 0 & 0 & G & 0 & 0 \\ \hline B_w & B_w & B_w & 0 & 0 & 0 & \beta_{ww} & \beta_{w\mathrm{Na}} \\ B_{\mathrm{Na}} & B_{\mathrm{Na}} & B_{\mathrm{Na}} & 0 & 0 & 0 & \beta_{\mathrm{Na}w} & \beta_{\mathrm{NaNa}} \end{array}\right] \left[\begin{array}{c} \delta\epsilon_{11} \\ \delta\epsilon_{22} \\ \delta\epsilon_{33} \\ 2\,\delta\epsilon_{12} \\ 2\,\delta\epsilon_{23} \\ 2\,\delta\epsilon_{13} \\ \hline \delta m_{wS} \\ \delta m_{\mathrm{Na}S} \end{array}\right]. \tag{B.12}$$

The elastic–plastic matrix form is obtained from (B.9) by mimicking (B.12).

Appendix C. Finite element matrices $\mathbb{C}^e$ and $\mathbb{K}^e$

$$\mathbb{C}^e = \left[\begin{array}{cccccccc} \mathbf{0} & \mathbf{0} & \mathbf{0} & \mathbf{0} & \mathbf{0} & \mathbf{0} & \mathbf{0} & \mathbf{0} \\ \mathbf{C}^e_{pu} & \mathbf{0} & \mathbf{0} & \mathbf{0} & \mathbf{0} & \mathbf{0} & \mathbf{0} & \mathbf{0} \\ \mathbf{0} & \mathbf{0} & \mathbf{C}^e_{c_{\mathrm{Na}}c_{\mathrm{Na}}} & \mathbf{0} & \mathbf{0} & \mathbf{C}^e_{c_{\mathrm{Na}}m_w} & \mathbf{C}^e_{c_{\mathrm{Na}}m_{\mathrm{Na}}} & \mathbf{0} \\ \mathbf{0} & \mathbf{0} & \mathbf{0} & \mathbf{C}^e_{c_{\mathrm{K}}c_{\mathrm{K}}} & \mathbf{0} & \mathbf{C}^e_{c_{\mathrm{K}}m_w} & \mathbf{C}^e_{c_{\mathrm{K}}m_{\mathrm{Na}}} & \mathbf{0} \\ \mathbf{0} & \mathbf{0} & \mathbf{0} & \mathbf{0} & \mathbf{C}^e_{c_{\mathrm{Cl}}c_{\mathrm{Cl}}} & \mathbf{C}^e_{c_{\mathrm{Cl}}m_w} & \mathbf{C}^e_{c_{\mathrm{Cl}}m_{\mathrm{Na}}} & \mathbf{0} \\ \mathbf{0} & \mathbf{0} & \mathbf{0} & \mathbf{0} & \mathbf{0} & \mathbf{C}^e_{m_wm_w} & \mathbf{0} & \mathbf{0} \\ \mathbf{0} & \mathbf{0} & \mathbf{0} & \mathbf{0} & \mathbf{0} & \mathbf{0} & \mathbf{C}^e_{m_{\mathrm{Na}}m_{\mathrm{Na}}} & \mathbf{0} \\ \mathbf{0} & \mathbf{0} & \mathbf{0} & \mathbf{0} & \mathbf{0} & \mathbf{0} & \mathbf{0} & \mathbf{0} \end{array}\right], \tag{C.1}$$

$$\mathbb{K}^e = \begin{bmatrix} \mathbf{K}^e_{uu} & \mathbf{K}^e_{up} & \mathbf{0} & \mathbf{0} & \mathbf{0} & \mathbf{K}^e_{um_w} & \mathbf{K}^e_{um_{\mathrm{Na}}} & \mathbf{0} \\ \mathbf{0} & \mathbf{K}^e_{pp} & \mathbf{K}^e_{pc_{\mathrm{Na}}} & \mathbf{K}^e_{pc_K} & \mathbf{K}^e_{pc_{\mathrm{Cl}}} & \mathbf{0} & \mathbf{0} & \mathbf{K}^e_{p\phi} \\ \mathbf{0} & \mathbf{K}^e_{c_{\mathrm{Na}}p} & \mathbf{K}^e_{c_{\mathrm{Na}}c_{\mathrm{Na}}} & \mathbf{K}^e_{c_{\mathrm{Na}}c_{\mathrm{K}}} & \mathbf{K}^e_{c_{\mathrm{Na}}c_{\mathrm{Cl}}} & \mathbf{0} & \mathbf{0} & \mathbf{K}^e_{c_{\mathrm{Na}}\phi} \\ \mathbf{0} & \mathbf{K}^e_{c_Kp} & \mathbf{K}^e_{c_Kc_{\mathrm{Na}}} & \mathbf{K}^e_{c_Kc_K} & \mathbf{K}^e_{c_Kc_{\mathrm{Cl}}} & \mathbf{0} & \mathbf{0} & \mathbf{K}^e_{c_K\phi} \\ \mathbf{0} & \mathbf{K}^e_{c_{\mathrm{Cl}}p} & \mathbf{K}^e_{c_{\mathrm{Cl}}c_{\mathrm{Na}}} & \mathbf{K}^e_{c_{\mathrm{Cl}}c_K} & \mathbf{K}^e_{c_{\mathrm{Cl}}c_{\mathrm{Cl}}} & \mathbf{0} & \mathbf{0} & \mathbf{K}^e_{c_{\mathrm{Cl}}\phi} \\ \mathbf{K}^e_{m_wu} & \mathbf{0} & \mathbf{K}^e_{m_wc_{\mathrm{Na}}} & \mathbf{K}^e_{m_wc_{\mathrm{K}}} & \mathbf{K}^e_{m_wc_{\mathrm{Cl}}} & \mathbf{K}^e_{m_wm_w} & \mathbf{K}^e_{m_wm_{\mathrm{Na}}} & \mathbf{0} \\ \mathbf{K}^e_{m_{\mathrm{Na}}u} & \mathbf{0} & \mathbf{K}^e_{m_{\mathrm{Na}}c_{\mathrm{Na}}} & \mathbf{K}^e_{m_{\mathrm{Na}}c_{\mathrm{K}}} & \mathbf{K}^e_{m_{\mathrm{Na}}c_{\mathrm{Cl}}} & \mathbf{K}^e_{m_{\mathrm{Na}}m_w} & \mathbf{K}^e_{m_{\mathrm{Na}}m_{\mathrm{Na}}} & \mathbf{0} \\ \mathbf{0} & \mathbf{0} & \mathbf{K}^e_{\phi c_{\mathrm{Na}}} & \mathbf{K}^e_{\phi c_{\mathrm{K}}} & \mathbf{K}^e_{\phi c_{\mathrm{Cl}}} & \mathbf{0} & \mathbf{0} & \mathbf{K}^e_{\phi\phi} \end{bmatrix}. \tag{C.2}$$

In the expressions below, the free indices k and l take values in $\{\mathrm{Na},\mathrm{K},\mathrm{Cl}\}$ and k' and l' in $\{w,\mathrm{Na}\}$. The non-zero components of the generalized diffusion matrix are

$$\begin{aligned} &\mathbf{C}^e_{c_kc_k} = \int_{V^e} \mathbf{N}_c^{\mathrm{T}} n_W \mathbf{N}_c \,\mathrm{d}V^e, \qquad \mathbf{C}^e_{m_{k'}m_{k'}} = \int_{V^e} \mathbf{N}_m^{\mathrm{T}} \frac{1}{T_{k'k'}} \mathbf{N}_m \,\mathrm{d}V^e, \\ &\mathbf{C}^e_{c_km_w} = -\int_{V^e} \mathbf{N}_c^{\mathrm{T}} \frac{c_{kW}}{\rho_w} \mathbf{N}_m \,\mathrm{d}V^e, \qquad \mathbf{C}^e_{pu} = \int_{V^e} \mathbf{N}_p^{\mathrm{T}} \operatorname{tr} \mathbf{B}_u \,\mathrm{d}V^e, \\ &\mathbf{C}^e_{c_km_{\mathrm{Na}}} = \int_{V^e} \mathbf{N}_c^{\mathrm{T}} \frac{1}{\rho_{\mathrm{Na}}} \left((I_{\mathrm{Na}k} - c_{kW}) - (I_{Kk} - c_{kW}) \frac{v_K^{(M)}}{v_{\mathrm{Na}}^{(M)}} \right) \mathbf{N}_m \,\mathrm{d}V^e. \end{aligned} \tag{C.3}$$

As for the generalized stiffness matrix,

$$\begin{aligned} &\mathbf{K}^e_{uu} = \int_{V^e} \mathbf{B}_u^{\mathrm{T}} \mathbf{D}_{uu} \mathbf{B}_u \,\mathrm{d}V^e, \qquad \mathbf{K}^e_{up} = -(\mathbf{C}^e_{pu})^{\mathrm{T}}, \\ &\mathbf{K}^e_{c_kc_l} = \int_{V^e} \nabla N_c^{\mathrm{T}} n_W (I_{kl} - c_{kW}) D_l^* \nabla N_c \,\mathrm{d}V^e, \\ &\mathbf{K}^e_{pp} = \int_{V^e} \nabla N_p^{\mathrm{T}} k_{WW} \nabla N_p \,\mathrm{d}V^e, \\ &\mathbf{K}^e_{c_kp} = \int_{V^e} \nabla N_c^{\mathrm{T}} \sum_{l=\mathrm{Na},\mathrm{K},\mathrm{Cl}} (I_{kl} - c_{kW}) k^d_{lW} \nabla N_p \,\mathrm{d}V^e, \\ &\mathbf{K}^e_{pc_k} = \int_{V^e} \nabla N_p^{\mathrm{T}} \frac{k^d_{Wk}}{c_{kW}} \frac{RT}{v_k^{(M)}} \nabla N_c \,\mathrm{d}V^e, \\ &\mathbf{K}^e_{\phi\phi} = \int_{V^e} \nabla N_\phi^{\mathrm{T}} \boldsymbol{\sigma}_e \nabla N_\phi \,\mathrm{d}V^e, \\ &\mathbf{K}^e_{c_k\phi} = \int_{V^e} \nabla N_c^{\mathrm{T}} \sum_{l=\mathrm{Na},\mathrm{K},\mathrm{Cl}} (I_{kl} - c_{kW}) k^d_{le} \nabla N_\phi \,\mathrm{d}V^e, \\ &\mathbf{K}^e_{\phi c_k} = \int_{V^e} \nabla N_\phi^{\mathrm{T}} n_W u_k^* \operatorname{sgn} \zeta_k \frac{RT}{v_k^{(M)}} \nabla N_c \,\mathrm{d}V^e, \\ &\mathbf{K}^e_{m_{k'}u} = \int_{V^e} \mathbf{N}_m^{\mathrm{T}} \sum_{l'=w,\mathrm{Na}} \frac{T_{k'l'}}{T_{k'k'}} \mathbf{D}_{l'u} \mathbf{B}_u \,\mathrm{d}V^e, \\ &\mathbf{K}^e_{um_{k'}} = \int_{V^e} \mathbf{B}_u^{\mathrm{T}} \mathbf{D}_{uk'} \mathbf{N}_m \,\mathrm{d}V^e, \\ &\mathbf{K}^e_{m_{k'}m_{l'}} = \int_{V^e} \mathbf{N}_m^{\mathrm{T}} \sum_{n'=w,\mathrm{Na}} \frac{T_{k'n'}}{T_{k'k'}} D_{n'l'} \mathbf{N}_m \,\mathrm{d}V^e, \\ &\mathbf{K}^e_{m_{k'}c_l} = \int_{V^e} \mathbf{N}_m^{\mathrm{T}} \sum_{n'=w,\mathrm{Na}} \frac{T_{k'n'}}{T_{k'k'}} \iota_{ln'} \mathbf{N}_c \,\mathrm{d}V^e, \end{aligned} \tag{C.4}$$

where $\iota_{lw} = RT/(m_w^{(M)} c_{wW}) \times v_w^{(M)}/v_l^{(M)}$ and $\iota_{l\mathrm{Na}} = RT/(m_{\mathrm{Na}}^{(M)} c_{lW}) \times \jmath_l$ with $\jmath_{\mathrm{Na}} = -1$, $\jmath_{\mathrm{K}} = 1$, $\jmath_{\mathrm{Cl}} = 0$. For associative plasticity, $\mathbf{D}_{mu} = \mathbf{D}_{um}^{\mathrm{T}}$, and then $\mathbf{K}_{mu}^{e} = (\mathbf{K}_{um}^{e})^{\mathrm{T}}$, for $m = m_w$, m_{Na}.

The contribution of the element e to the vector F_e^{surf} of surface data is defined from the weak form as,

$$\mathbb{F}_e^{\mathrm{surf}} = \begin{bmatrix} \int_{\partial V^e} \mathbf{N}_u^{\mathrm{T}} \boldsymbol{\sigma} \cdot \hat{\mathbf{n}} \, \mathrm{d}S \\ -\int_{\partial V^e} \mathbf{N}_p^{\mathrm{T}} \mathbf{J}_W \cdot \hat{\mathbf{n}} \, \mathrm{d}S \\ \int_{\partial V^e} \mathbf{N}_c^{\mathrm{T}} \boldsymbol{\alpha}_{\mathrm{Na}} \cdot \hat{\mathbf{n}} \, \mathrm{d}S \\ \int_{\partial V^e} \mathbf{N}_c^{\mathrm{T}} \boldsymbol{\alpha}_{\mathrm{K}} \cdot \hat{\mathbf{n}} \, \mathrm{d}S \\ \int_{\partial V^e} \mathbf{N}_c^{\mathrm{T}} \boldsymbol{\alpha}_{\mathrm{Cl}} \cdot \hat{\mathbf{n}} \, \mathrm{d}S \\ \mathbf{0} \\ \mathbf{0} \\ -\int_{\partial V^e} \mathbf{N}_\phi^{\mathrm{T}} \mathbf{I}_{\mathrm{e}W} \cdot \hat{\mathbf{n}} \, \mathrm{d}S \end{bmatrix}, \tag{C.5}$$

where $\boldsymbol{\alpha}_k$, $k = \mathrm{Na}, \mathrm{K}, \mathrm{Cl}$, is defined by (5.2).

The contribution of the element e to the vector $F_e^{\mathrm{int+grav}}$ of internal forces and gravity forces is defined from the weak form as,

$$\mathbb{F}_e^{\mathrm{int+grav}} = \begin{bmatrix} \int_{V^e} \mathbf{B}_u^{\mathrm{T}} \boldsymbol{\sigma} \, \mathrm{d}V^e - \int_{V^e} \mathbf{N}_u^{\mathrm{T}} (\rho \mathbf{g}) \, \mathrm{d}V^e \\ \int_{V^e} \mathbf{N}_p^{\mathrm{T}} \operatorname{div} \mathbf{v}_{\mathbf{S}} - \nabla \mathbf{N}_p^{\mathrm{T}} \mathbf{J}_W \, \mathrm{d}V^e \\ \int_{V^e} \mathbf{N}_c^{\mathrm{T}} \beta_{\mathrm{Na}} + \nabla \mathbf{N}_c^{\mathrm{T}} \boldsymbol{\alpha}_{\mathrm{Na}} \, \mathrm{d}V^e \\ \int_{V^e} \mathbf{N}_c^{\mathrm{T}} \beta_{\mathrm{K}} + \nabla \mathbf{N}_c^{\mathrm{T}} \boldsymbol{\alpha}_{\mathrm{K}} \, \mathrm{d}V^e \\ \int_{V^e} \mathbf{N}_c^{\mathrm{T}} \beta_{\mathrm{Cl}} + \nabla \mathbf{N}_c^{\mathrm{T}} \boldsymbol{\alpha}_{\mathrm{Cl}} \, \mathrm{d}V^e \\ \int_{V^e} \mathbf{N}_m^{\mathrm{T}} \left(\frac{1}{T_w} \frac{\delta m_{wS}}{\delta t} - (\bar{\mu}_{wW} - \bar{\mu}_{wS}) - \frac{T_{w\mathrm{Na}}}{T_w} (\bar{A}_W - \bar{A}_S) \right) \mathrm{d}V^e \\ \int_{V^e} \mathbf{N}_m^{\mathrm{T}} \left(\frac{1}{T_{\mathrm{Na}}} \frac{\delta m_{\mathrm{Na}S}}{\delta t} - \frac{T_{\mathrm{Naw}}}{T_{\mathrm{Na}}} (\bar{\mu}_{wW} - \bar{\mu}_{wS}) - (\bar{A}_W - \bar{A}_S) \right) \mathrm{d}V^e \\ \int_{V^e} \nabla \mathbf{N}_\phi^{\mathrm{T}} \cdot (-\mathbf{I}_{\mathrm{e}W}) \, \mathrm{d}V^e \end{bmatrix}, \tag{C.6}$$

where

$$\beta_k = n_W \frac{\delta c_{kW}}{\delta t} + \sum_{l \in S^{\leftrightarrow}} (I_{kl} - c_{kW}) \frac{\delta v_{lS}}{\delta t}, \quad k = \mathrm{Na}, \mathrm{K}, \mathrm{Cl}. \tag{C.7}$$

Wiggles due to advective terms are cured by a SUPG method as in GL.

Appendix D. Dependent variables

D.1. Solid phase

The mass-contents m_{kS}, $k = c$, Cl, in the solid phase are constant while m_{wS} and $m_{\mathrm{Na}S}$ are primary variables and $m_{\mathrm{K}S}$ is deduced from $m_{\mathrm{Na}S}$ by the electroneutrality condition. The volume V is deduced from the computed strain field as $V = V_0(1 + \operatorname{tr} \epsilon)$. The volume-contents and volume fractions are obtained directly from their definitions, namely $v_{kS} = m_{kS}/\rho_k$ and $n_{kS} = m_{kS}/\rho_k \times (V_0/V)$, for any $k \in S$. The elastic molar fractions x_{kS}^{el}, $k = w$, Na, K, are obtained from the elastic masses m_{wS}^{el} delivered together with the masses m_{kS} by the constitutive equations.

D.2. Fluid phase

Since the ionic concentrations are primary variables, c_{wW} can be obtained by $\sum_{k\in W} c_{kW} = 1$. The molar fractions x_{kW}, $k \in W$, are obtained from (2.5). The rate Eq. (A.9) of GL for n_W, which involves only primary variables, may be integrated for n_W. The ionic volume fractions and volume-contents follow from (2.5).

The apparent densities of the species ρ^{kK}, phases ρ^K and mixture ρ result from the knowledge of the volume fractions.

Appendix E. Comparison with hydrogeological approaches

The mass balance equations of ionic species (2.17) may be rewritten to highlight the fact that, with respect to the solid phase, these species move by diffusion and advection by the water phase. For the ionic species $k \in W^{\pm}$,

$$n_W \frac{\delta c_{kW}}{\delta t} + \sum_{m\in W^{\pm}} \nabla c_{mW} \cdot \mathbf{v}^{\mathrm{adv}}_{km} - \sum_{l\in W^{\pm}} (I_{kl} - c_{kW}) \operatorname{div}(n_W D^*_l \nabla c_{lW}) = \sum_{l\in W^{\pm}} (I_{kl} - c_{kW})(k^d_{lW}\Delta p_W + k^d_{le}\Delta\phi_W) - \sum_{l\in S^{\leftrightarrow}} (I_{kl} - c_{kW}) \frac{\delta v_{lS}}{\delta t}, \tag{E.1}$$

with the approximative [5] advective velocities $\mathbf{v}^{\mathrm{adv}}_{km}$, $m \in W^{\pm}$,

$$\mathbf{v}^{\mathrm{adv}}_{km} = \left(\mathbf{J}_W - \sum_{l\in W} \mathbf{J}^d_{lW}\right) I_{km} - \sum_{l\in W} (I_{kl} - c_{kW}) \left(\frac{\partial k^d_{lW}}{\partial c_{mW}} \nabla p_W + \frac{k^d_{le}}{c_{lW}} \nabla\phi_W I_{lm}\right). \tag{E.2}$$

A comparison of the present approach using thermodynamic potentials with models used in hydrogeology is presented briefly in GL in the context of homoionic clays, their Section 3.3. Worth to be stressed are the following points:

- Hydrogeology mainly concerned with pollutant transport assumes a rigid solid phase while a deformable elastic–plastic solid phase is developed here.
- Mass transfers/reactions arise naturally in the present framework as an exchange between the two phases. They appear in hydrogeology as source terms through absorption/desorption isotherms. Our transfers are endowed with a characteristic time while the absorption in hydrogeology is usually instantaneous. The reversibility and irreversibility properties of the transfers are linked to plasticity. In hydrogeology, different isotherms in absorption and desorption need to be assumed to introduce irreversibility. In both approaches, transfers introduce a retardation factor in the advection-diffusion equations.

Note that, in the actual finite element computations, the advective velocities are simplified to $\mathbf{J}_W$, which has the additional advantage of easing the treatment of electroneutrality.

References

Acar, Y.B., Gale, R.J., Hamed, J., Putnam, G., 1991. Acid/base distribution in electrokinetic soil processing. Soils Geology and Foundations, Geotechnical Engineering, Bull. Transportation Research Record 1288, 23–34.

[5] The approximation comes from the fact that in the calculation of the advective velocities the dependence of n_W in concentrations has been neglected.

Barbour, S.L., Fredlund, D.G., 1989. Mechanisms of osmotic flow and volume change in clay soils. Can. Geotech. J. 26, 551–562.
Bataille, J., Kestin, J., 1977. Thermodynamics of mixtures. J. Non-Equil. Thermodyn. 2, 49–65.
Bennethum, L.S., Cushman, J.H., 1999. Coupled solvent and heat transport of a mixture of swelling porous particles and fluids: single time-scale problem. Transport Porous Med. 36, 211–244.
Di Maio, C., 1996. Exposure of bentonite to salt solution: osmotic and mechanical effects. Géotechnique 46 (4), 695–707.
Di Maio, C., 1998. Discussion on Exposure of bentonite to salt solution: osmotic and mechanical effects. Géotechnique 48 (3), 433–436.
Di Maio, C., Fenelli, G., 1997. Influenza delle interazioni chimico-fisiche sulla deformabilità di alcuni terreni argillosi. Riv. Ital. Geotec. 1, 695–707.
Di Maio, C., Onorati, R., 1999. Prove di laboratorio: influenza della compozione del liquido di cella. Rendiconti del XX Convegno Nazionale di Geotecnica, Parma, pp. 87–94.
Eringen, A.C., Ingram, J.D., 1965. A continuum theory for chemically reacting media—I. Int. J. Engng. Sci. 3, 197–212.
Farrar, D.M., Coleman, J.D., 1967. The correlation of surface area with other properties of nineteen British clay soils. J. Soil Sci. 18 (1), 118–124.
Gajo, A., Loret, B., 2003. Finite element simulations of chemo-mechanical coupling in elastic–plastic homoionic expansive clays. Comput. Methods Appl. Mech. Engng. 192, 3489–3530.
Gajo, A., Loret, B., Hueckel, T., 2002. Electro-chemo-mechanical couplings in saturated porous media: elastic–plastic behaviour of heteroionic expansive clays. Int. J. Solids Struct. 39, 4327–4362.
Haase, R., 1990. Thermodynamics of Irreversible Processes. Dover Publications, New York.
Hueckel, T., 1992. Water-Mineral Interaction in Hygro-Mechanics of Clays Exposed to Environmental Loads: a Mixture Approach. Can. Geotech. J. 29, 1071–1086.
Huyghe, J.M., Janssen, J.D., 1999. Thermo-chemo-electro-mechanical formulation of saturated charged porous solids. Transport Porous Med. 34 (1–3), 129–141.
Kaczmarek, M., Hueckel, T., 1998. Chemo-mechanical consolidation of clays: analytical solutions for a linearized one-dimensional problem. Transport Porous Med. 1330, 1–26.
Levenston, M.E., Eisenberg, S.R., Grodzinsky, A.J., 1998. A variational formulation for coupled physicochemical flows during finite deformations of charged porous media. Int. J. Solids Struct. 35, 4999–5019.
Loret, B., Gajo, A., 2004. Multi-phase multi-species mixtures. In: Loret, B., Huyghe, J.M. (Eds.), Chemo-mechanical Couplings in Geomechanics and Biomechanics, Cism Course 249, Springer-Verlag, Wien, New York, pp. 149–164, in press.
Loret, B., Gajo, A., Simões, F.M., 2004. A note on the dissipation due to generalized diffusion with electro-chemo-mechanical couplings in heteroionic clays, European J. Mech. A/Solids, in revised form.
Loret, B., Hueckel, T., Gajo, A., 2002. Chemo-mechanical coupling in saturated porous media: elastic–plastic behaviour of homoionic expansive clays. Int. J. Solids Struct. 39, 2773–2806.
Malusis, M.A., Shackelford, C.D., 2002. Chemico-osmotic efficiency of a geosynthetic clay liner. J. Geotech. Engng. Div., Trans. ASCE 128 (12), 97–106.
Malusis, M.A., Shackelford, C.D., 2003. Coupling effects during steady-state solute diffusion through a semi-permeable clay membrane. Environ. Sci. Technol. 36 (6), 1312–1319.
Manassero, M., Dominijanni, A., 2003. Modelling the osmosis effect on solute migration through porous media. Géotechnique 53 (5), 481–492.
Mitchell, J.K., 1993. Fundamentals of Soil Behavior, 2nd ed. J. Wiley & Sons, Chichester.
Murad, M.A., 1999. Thermo-mechanical model for hydration swelling in smectitic clays. Int. J. Numer. Anal. Methods Geomech. 27 (7), Part I: 673–696, Part II: 697–720.
Sherwood, J.D., 1993. Biot poroelasticity of a chemically active shale. Proc. R. Soc. Lond. 440, 365–377.
Simo, J., Hughes, T.J.R., 1987. General return mapping algorithms for rate-independent plasticity. In: Desai, C.S. et al. (Eds.), Constitutive Laws for Engineering Materials: Theory and Applications. Elsevier Science Publ. Co, pp. 221–231.
Simon, B.R., Kaufman, M.V., Liu, J., Baldwin, A.L., 1998. Porohyperelastic-transport-swelling theory, material properties and finite element models for large strains. Int. J. Solids Struct. 35, 5021–5031.
Smith, D., 2000. One-dimensional contaminant transport through a deforming porous medium: theory and a solution for a quasi-steady-state problem. Int. J. Numer. Anal. Meth. Geomech. 24, 693–722.
Yeung, A.T., 1990. Electrokinetic barrier to contaminant transport through compacted clay, Ph.D. Dissertation, University of California, Berkeley, p. 260.
Yeung, A.T., Datla, S., 1995. Fundamental formulation of electrokinetic extraction of contaminants from soil. Can. Geotech. J. 32, 569–583.